Computer simulation by quantum mechanical time dependent wave packet method especially for atom / molecule – solid surface interaction

*G. Varga**

Budapest University of Technology and Economics, Department of Physics, Budafoki út. 8, Budapest, Hungary, H-1111

Thermal energy atomic scattering on solid surfaces (TEAS) is a useful experimental method to obtain information about the structure, disorders and phonon-spectra of the solid surface. The probe particles (usually He atoms) could spend relatively long time near the solid surface at the interaction region. Dynamics of these interaction processes can not be investigated directly at present. However, an appropriate physical model of the interaction fitted to the intensity distribution of the scattering may be suitable to investigate theoretically the interaction processes by computer simulation. The present work emphasises this computer simulation method (CSM). For an actual CSM an appropriate experimental method at the detector region (TEAS) is required. Moreover a theoretical model for the TEAS (e.g. a one particle quantum mechanical wave packet model governed by the time dependent Schrödinger equation (TDSE)) and a numerical method for solving the TDSE are necessary.

The state functions of the consecutive time steps provide enough information as an animation to describe the dynamics of the interaction processes. The animation means subsequent snapshots of e.g. probability density function (PDF) in rapid succession. The sequence of these snapshots provides a movie of the PDF time evolution.

Applications, physical models, numerical solution procedures and simulation techniques of time dependent wave packet method (TDWP) are overviewed in present contribution, especially for the case of TEAS and molecular beam scattering (MBS). Several relevant applications of TDWP method - in the case of TEAS - are discussed (scattering on ordered, stepped and adsorbed surfaces, intensity distribution as a function of transfer width, resonant adsorption and trapping, classical and quantum chaos, scattering from vibrating surface). Preliminary result of quantum chaos of TEAS is presented first. Theoretical and computational background (TDWP and coupled channel method (CC)) as well as applications (diffraction probability, sticking probability, dissociative adsorption, steering effect, inelastic channels) of six dimensional molecule/surface dynamics calculations are shown.

Keywords: Atom – solid interactions, scattering, diffraction; Computer simulation; Quantum effects; Rhodium; Surface structure; Single crystal; Resolution; Transfer width; Numerical solution to Schroedinger equation; Wave packet method; Molecule – solid interaction; Quantum chaos; Molecular dynamics; Animation techniques; Split operator method; TEAS; MBS

E-mail address: vargag@phy.bme.hu (G. Varga).

* Home Page: http://goliat.eik.bme.hu/~vargag/.

1. Introduction

Thermal energy atomic scattering on solid surfaces (TEAS) is an efficient method to explore the surface topology, phonon spectra, surface disorders and the probe particle - solid surface interaction. Molecular beam scattering (MBS) is suitable to explore the molecule - solid surface reactions. TEAS and MBS usually demand quantum mechanical model to describe the physical phenomena. Classical and semi-classical models are also applied in the literature to characterise TEAS and MBS. Since, the interaction of the atom (e.g. He) – solid surface system changes abruptly near the classical turning point the classical trajectories are washed out. This fact supports the application of an appropriate quantum mechanical model. The probe particles of larger mass and higher energy bring about weaker quantum effect and the semi-classical and classical models come to the fore.

The traditional quantum mechanical models of TEAS suppose periodical solid surfaces. A successful and simple quantum mechanical model, the so-called hard corrugated wall model (HCW) was developed by García [1]. The probe particle interaction potential is zero above the surface but infinite at the corrugated surface. The state function at the solid surface is equal to zero due to the infinite potential wall. According to this assumption the solution of a complex linear system of equations will lead to the diffraction pattern at the detector region.

García's method has been improved by Varga et al. and Stoll et al [2-4]. The convergence and the stability have also been improved. The symmetry of the solid surface has been considered [5], too, that led to an efficient inverse scattering algorithm [6-7]. An integral equation solution method has been introduced by Salanon and Armand [8].

The soft corrugated wall model was the next quantum mechanical model. Executing the numerical solution, the time independent Schrödinger equation was applied to a series of reciprocal lattices of the solid surfaces. This method provided a system of close-coupled differential equations. Its solution gives the scattering amplitude (CCGM method [9]). In the case of smooth surfaces (e.g. certain metal surfaces) a perturbation theory – the so-called distorted Born approximation - is also an efficient method [10]. The details and further references of TEAS theory and experiments can be found in [11-12].

A real surface contains different disorders, e.g. adatoms, vacancies, steps. The surface disorders deform the perfect periodicity. This fact hinders the application of the above mentioned traditional methods. The wave packet method is appropriate to eliminate this problem. In the framework of the time dependent wave packet method (TDWP) the atomic/molecule beam is described as an ensemble of independent particles represented by appropriate Gaussian wave packet**.** The wave packet velocity and spread ensure the right average beam energy and the monochromaticity, respectively. The surface might be disordered because the wave packet time propagation is governed by time dependent Schrödinger equation (TDSE) and the surface periodicity is not exploited in the numerical solution. The physical quantities can be computed from the state function. (See details in the Appendix.) It is a relevant property of TDWP method that the time evolution of the physical phenomena is received by the wave packet propagation. As a result of that, during the process the state of the atomic beam is known beyond the detector region, too. By the TDWP method one can also calculate the dynamics of the interaction region near the classical turning point where the measurement of the atomic beam state is impossible nowadays.

Section 2 reviews some research areas of the TDWP method. The numerical tools for the TDWP method are discussed in section 3. In the subsequent section the computer animation as a computer simulation method is introduced. The TDWP method - in the case of TEAS and MBS - is described in section 5 and in section 6, respectively, with several applications. The conclusions are shown in section 7.

2. Recent applications and development of TDWP method

It is important to mention the details of the different applications are not treated thoroughly in this section, the reader is referred to the references.

Recently TDWP has been used for the description of *reactive scattering*, to calculate the microcanonical cumulative reaction probability and probabilities of molecular transitions in time dependent fields, or to decouple reactant and product parts of the wave function in state to state reactive scattering calculations. An accurate time dependent wave packet calculation for the O(D)+DCl reaction is carried out employing a potential energy surface [13]. Apparent differences are found in the energy-dependence of reaction probability and the magnitude of rate constants between the O(D)+DCl reaction and its isotopic O(D)+HCl reaction [14]. These differences are attributed mainly to kinematic effect. Classical and quantum dynamics computations on the collinear potential energy surface for the reaction of Li with H_2 have been executed by Clarke and co-workers [15]. The specific features of the potential are analysed for some indicative configurations and classical trajectory calculations are carried out for a special collinear arrangement. In the case of collinear arrangement the quantum time dependent wave packet calculations have also been performed and the two sets of results are found to be in rather good accord with each other. C. Zhang and co-workers [16] applied time dependent quantum wave packet calculation for the HD+CN reaction. That has been carried out on a new potential energy surface with the potential averaged five dimensional model. Discrete variable representations for radial co-ordinate and a renormalized angular quadrature scheme are applied in the wave packet propagation in order to save computer memory. Domenico and co-workers [17] presented a time dependent wave packet approach to compute the reaction and collision-induced dissociation probabilities for $H_2 + H_2$. It has been found that the method provides more accurate results than a time independent hyperspherical treatment. The time dependent quantum wave packet method has been applied by C. Zhang and co-workers [18] to study the dynamics of ion molecule reaction of $N^+ + H_2$ on special potential energy surface.

Atomic phenomena in *bichromatic laser fields* can be described by wave packet method as the atomic electron is modelled by wave packet [19]. The computation demands the solution of the one- and three-dimensional TDSE.

Ferrero and Robicheaux [20] presented a theory for the scattering of a *short electron pulse* from a molecular wave packet. They investigated the transition between two electronic states and showed how transition probabilities as a function of internal nuclear positions can be obtained. Pulsed electron beam can also be used to control the transition probabilities to different electronic levels by direct numerical solution of TDSE.

Nuclear wave packets are prepared by a chirped femtosecond laser pulse depending on the chirp parameter, exhibit different vibrational dynamics [21]. Using the potassium dimer it can be shown that the time-resolved photoelectron

spectroscopy is able to map the characteristics of the nuclear probability density and to distinguish densities obtained from excitations using differently chirped pulses. The numerical calculations provide the information about the uncertainties of wave packets, which can be directly obtained from the spectra.

3D wave packet calculations on the O_3 molecule have been performed the case, when the total angular momentum equals to zero [22]. The split operator propagator and the fast Fourier transform method in hyperspherical co-ordinates are used in order to follow the quantum dynamics of *photodissociation*. The effect of the finite lifetime of the excited state has been studied, in order to explain the disagreement between the theoretical calculations and experimental data.

Time dependent photodissociation resonances are investigated in the case of collinear CO_2 system using the wave packet method [23]. The excited- and ground-state wave packet behaviour caused by frequency-chirping of a femtosecond laser pulse in H_2 - photodissociation has been investigated using a time dependent method [24]. Control over wave packet processes is the foundation of laser control of chemical reaction dynamics. The critical stage in a chemical reaction occurs within 10^{-12} s. After femtosecond laser technology had emerged it was possible to manipulate and control molecular processes in this key stage. The most important task is to solve the coupled time dependent Schrödinger equations.

The *photoabsorption* spectra of the molecules HI and DI are computed using ab initio potential curves and transition dipole moments [25]. Partial absorption cross-sections and an excited spin-orbit state of iodine are calculated using the time dependent wave packet formalism as a function of the excitation energy. Good agreement with experimental data is obtained. The wave functions and potentials are represented on a set of equally spaced grid points and the Schrödinger equation is solved using the split-operator method.

Mahapatra and co-workers [26] investigated the *nonadiabatic wave packet dynamics* on the coupled electronic states of NO_2 based on new ab initio potential energy surfaces. The elements of the vibronic Hamiltonian are weakly varying function of the nuclear co-ordinates and the kinetic energy operator can be taken as diagonal.

Sweeney and De Vries [27] applied the split operator method solution of TDSE to two-dimensional *Rutherford scattering* and the wave function was visualised as a function of time.

De Raedt [28-30] focused on simulating the quantum mechanical motion of *electrons in nano-scale devices*. Supplemented by computer animation techniques the simulation provides a clear insight into the physical behaviour. Aharonov-Bohm effect has been simulated by wave packet method, too.

Andersson and Stenholm [31] investigated the cooling and trapping techniques for atoms allowing the fabrication of genuinely microscopic *quantum wires and dots for individual particles*. The physical feature of a structure was discussed and it was illustrated with wave packet simulations.

Márk and his co-workers [32-35] executed thorough computer simulation of *scanning tunneling microscopy* (STM) experiments to Carbon nanotubes. Three dimensional wave packet method has been applied to explore the dynamics of the electron tunneling between the realistic STM tip and the Carbon nanotubes. The time propagation of the probability density function is rendered in the nanotube as a computer animation and as the electron dwell time distribution. The simulation results were compared to the experimental ones, too.

Further fruitful applications of TDWP method are the investigation of *atom/molecule solid surface interactions* by TEAS and MBS. Details can be seen in section 5 and 6, respectively.

3. Numerical solution methods for TDWP method

If the quantum system is small and if it contains dissociative or tunneling co-ordinates the grid method is very convenient to use direct procedure which avoids state expansion. Nowadays six-dimensional computations can be executed in several cases. Of course the degree of freedom depends on the physical situation that can be handled without super computer. For atom/molecule - solid surface scattering and interaction, grid methods can be extremely useful. The methods are accurate, suitable for investigation of complex systems as is shown in section 2. The numerical procedure of the solution of Schrödinger equation can be divided into the following steps:

(a) *An appropriate initial wave function has to be chosen.* Average energy and energy spread of the atomic beam must be considered. It is a good idea to choose a Gaussian wave packet for determining the intensity distribution of TEAS. However, the composition of the initial wave packet is a crucial question that depends on the physical phenomena, which we want to investigate. For example, if the dynamics of diatomic molecule scattering has to be analyzed, the initial wave function should be a sum of the incoming plane waves at the detector region where the particle moves as a free one. This is why a plane wave should contain the product of the following functions: a plane wave perpendicular to the surface, a function describing parallel translational motion, a vibrational wave function for molecule in the appropriate rovibrational state and spherical harmonic function of the appropriate rotational state. This ansatz provides the possibility to describe rovibrational and rotational probabilities of different states, which are identified by certain quantum numbers. Namely, a right initial wave function should span the physical space of the processes. This type of initial wave function construction speeds up the convergence of the numerical procedure, as well as decreases the computational effort.

(b) *Boundary condition has to be chosen.* Large enough subspace has to be chosen in order to the wave function should become zero at boundary points under the whole physical process. If it is not realizable - e.g. because of the computer memory is out of – absorbing [60][62] or cutting techniques [93][148] for the wave function are required.

(c) *A method has to be applied to construct the Hamilton operator.* It can be calculated by finite difference method, finite element method and pseudo spectral method. The fast Fourier transformation (FFT) is an efficient pseudo spectral algorithm [36-39]. FFT demands periodical boundary condition, but the convergence speed is exponential in the number of terms. Unfortunately, the convergence of the finite difference method is only polynomial. The finite element method has good convergence characteristics and the boundary conditions can be built easily, however the computer code generation of the mesh is complicated [40-41].

(d) *One has to choose a time propagation approach.* The global operator scheme - e.g. Chebyshev scheme - determines the time propagator for a longer time interval [42-43]. These methods can be extremely accurate, however it is not recommended to time dependent interaction energy problems and for wave functions which occupy very small spectral range in relation to the spectral range of the grid. Chebysev scheme does not hold the

norm, does not conserve the energy and it is unstable for grid density. Finite difference scheme of the time propagator – the second order difference scheme (SOD) is the simplest – is based on Taylor series [44]. The SOD scheme holds the norm, conserves the energy, unstable for the grid density and time step. Split operator method (SPO) divides into two different parts the Hamiltonian [38][45-49]. First part is the kinetic energy and the second part is the interaction energy. The approximative formula contains pure kinetic energy and interaction energy terms. These non-mixed terms can be calculated efficiently as an algebraic operation in the momentum space (kinetic energy) and in the real space (interaction energy). Between the momentum space and the real space a vice-versa transformation is required (e.g. FFT). The short iterative Lánczos propagation (SIL) is based on generating a set of orthogonal polinomials lying within the subspace, which represents a finite polynomial approximation to the operator [50-52]. SIL holds the norm and conserves the energy, it is stable for grid density.

(e) *The error indication is a relevant task.* The computation accuracy can be controlled by the time symmetry of TDSE in the case of all methods. When one goes back to the time one should get back the starting wave function. The difference between the original initial wave function and the computed one can be measured by any norm - e.g. Eucledian norm – especially focusing on the phase error. Based on the above description of the different time propagation methods, other indicators can also be found. Chebysev method can be controlled by the norm of the wave function and the particle average energy. Since SOD method holds the unity of the wave function and conserves the energy, these physical quantities are not suitable to indicate the computation accuracy. However, SOD method is unstable for grid density. If the grid density is not large enough the method is divergent. Because the SPO method does not conserves the energy, the average energy as a function of time is a good indicator.

(f) *The wave function has to be analysed* to get the time propagation of the physical quantities (see appendix).

Further details of the numerical solution can be found in the following references: Gerber and co-workers [53], R. Kosloff [54], Billing [55], Leforester and co-workers [56] and Thaller [57].

3.1 Further development for numerical solution of TDWP method

Let us show some results that contain new and efficient numerical procedures. The predissociation dynamics of the vibrational eigenstates of hydrogen bromide ions in the first excited electronic states - that occurs via coupling to three repulsive states - has been investigated by direct solution of *four coupled 1D time dependent Schrödinger equations* [58]. The analysis shows multi-exponential decay for most of the predissociating vibrational states. The lifetime of these states decreases by several orders of magnitude. The split-operator method [38] as well as the integral equation method [59] have been used for determining the propagation of the wave functions. The absorbing boundary [60] is used to prevent the artificial reflection of the wave functions at the edge of the grid.

Dattoli and Mancho [61] exploited the formal properties of the evolution operator of Fokker-Planck and Schrödinger equations. Evolution operator is approximated with special forms *of Laguerre polynomials and Laguerre-based functions*. An advantage offered by the split operator method is that there is no explicit requirement of evaluating the Fourier transform of the initial function. The main disadvantage is that an iteration procedure is unavoidable.

Palao and Muga [62] developed a simple construction of *absorbing potentials* in the case of TDSE. Complex absorbing potentials are important auxiliary tools in TDWP method. The traditional role of the absorbing potentials is to elude too much computational efforts by avoiding spurious reflections at the edges of the finite „box" where the wave packet is enclosed. If periodic boundary conditions are imposed they also prevent the „transmission" to the other side of the box. The procedure of absorbing potential is based on adding a series of equal length complex square barriers and optimizing their real and imaginary parts to achieve maximum absorption at a selected set of momenta. The absorption widths obtained are better than other known functional forms for the important low momentum region. Summarily, Palao and Muga have proposed a method to construct optimised absorbing potentials by combining complex square barriers.

Jiang and co-workers [63] proposed two new propagation schemes of the *quantum time dependent self-consistent field equations* from a different point of view. If the state of the system under discussion is represented by a multiple-element vector wave function, a time independent quasi-Hamilton operator for the total system can be defined.

Nest and co-workers [64] applied the *mapped Fourier method* for scattering problems. The new scheme uses a non-equidistant grid point set. The key idea is to construct an adaptive grid, with a high grid-point density in regions where large momenta are expected. Numerical results are presented for scattering of Ar atomic wave packets from a Cu model surface.

Mikhailova and Pupyshev [65] have improved the accuracy of the *symmetric expansions* for the TDSE evolution *operator up to the fifth order* in time. This formula was applied to MBS. TEAS may be a further application of it.

Gollub and Richards [66] implemented a TDSE solver on *Parallel Computers* by space-splitting method [67] without spectral computations. The second order approximation of Laplacian resulted special tridiagonal matrices and their exponential functions have been computed to formulate for parallel computers efficiently.

A *pseudospectral method* for solving the time dependent Schrödinger equation in *spherical co-ordinates* is presented by Corey and Lemoine [68]. The translational kinetic energy operator is evaluated with Fourier transform. The angular dependence of the wave function is expanded on a two-dimensional grid in co-ordinate space and the angular part of the Laplace operator is evaluated by a *Gauss-Legendre-Fourier transform* between the co-ordinate and the conjugate angular momentum representation. Calculation was performed for H_2 molecule scattering on a frozen periodic surface.

Lemoine [69] published a numerical algorithm (the so-called *discrete Bessel transform*) and a FORTRAN 77 program of optimal cylindrical and spherical Bessel transforms satisfying bound state boundary conditions. The illustrative program applies the discrete Bessel transform to the eigenvalue calculation for two- and three-dimensional harmonic oscillator.

4. Computer animation

To exploit the computer simulation methods (CSM) computer animation of the physical quantities can be a useful tool. The animation means consecutive snapshots of the physical quantity as the time elapses. The manner of the

animation depends on the space dimension of the physical problem. A 2D problem can be rendered as a series of 3D snapshots. A 3D problem would demand 4D full graphical demonstration that is impossible. However, one can render snapshots of the 2D slices (window technique) in the space or snapshots of the isosurfaces (isosurface technique). Window technique might apply 2D rendering using a colour scale to show the distribution of the physical quantity or 3D rendering of 2D surfaces. Isosurface technique means that one can find the points in the 3D space where the physical quantities are equival to a given value. In the case of the isosurface technique relevant question is how to choose the isosurface value. For window technique and 3D snapshots some applications can be found in [70], viz., TEAS from 2D and 3D corrugated surfaces near the interaction and at the detector region considering the evolution of diffraction peaks and adsorption. Some picturesque computer animations can be looked at [71].

As researches show, the interactivity in human-computer connection is important [72]. Advancements in computer technology have allowed the development of human-appearing. Increased richness and anthropomorphism in interface design lead to computers becoming more influential during for making decision.

The animation techniques might become efficient in the case of inverse procedures, too. Murray-Smith analyses the problem of inverse techniques for dynamic simulation models [73]. These techniques allow computation of the time history of „inputs" needed to achieve a specified time history for a selected set of „outputs". In general terms, the available methods of inverse simulation may be numerical differentiation or iterative techniques. The iterative techniques are based upon numerical integration processes.

5. Atom scattering on surfaces

A relevant question is whether purely quantum mechanical, semi-classical or classical models have to be treated and the probe particle-surface coupling is considered or not. The type of the model depends on the physical processes and applications. In many cases it is enough to apply a frozen surface model when the coupling between the probe particle and the solid surface is not of primary interest. This situation might occur investigating surface structure, surface disorders and adsorption dynamics. (See details about molecule dynamics in section 6). However, if one would like to determine or explore the solid surface dynamics, the coupling of the probe atom-vibrating surface becomes relevant. In general, if the probe particle energy (or mass) is high enough classical or semiclassical models are acceptable. It is supported by the following computations: A semiclassical rainbow analysis of He-Cu(115) and Cu(117) is presented in [74]. This is based on a semiclassical approximation to S-matrix summing over all appropriate trajectories. The method of quantum trajectories proposed by de Broglie and Bohm is applied to study of atom diffraction on surfaces [75]. There is excellent agreement with results calculated by standard S matrix methods of scattering theory. De Broglie and Bohm quantum theory was solved numerically by the Heller's [76] method. Heller's approach is based on appropriate wave packet propagation.

The transition to the classical limit in atom-surface diffraction is studied using the de Broglie-Bohm causal formalism [77]. In order to achieve this limit, the mass of the probe particles have been increased in the case of scattering on Cu(110) surface. Quantum trajectories mimicked the classical intensity distribution.

5.1 Details to computations

The time dependent Schrödinger equation (TDSE) was solved numerically by Varga [78] using the seven split operator time step formula, that is more efficient than the standard three split operator one. This numerical solution procedure can handle the time dependent Hamilton operator, when the interaction energy and kinetic energy operators can be separated. The TDSE describes the atomic beam as a quantum ensemble of the independent particles. Let us consider the 3D time dependent Schrödinger equation:

$$i\hbar \frac{\partial \Psi(\mathbf{r},\mathrm{t})}{\partial \mathrm{t}} = H\,\Psi(\mathbf{r},\mathrm{t}), \quad H = -\frac{\hbar^2}{2m}\left(\frac{\partial^2}{\partial x^2}+\frac{\partial^2}{\partial y^2}+\frac{\partial^2}{\partial z^2}\right)+V(\mathbf{r},t)\,. \tag{1}$$

$\hbar$ is Planck constant divided by 2π, H is the Hamiltonian, (x,y,z) are Cartesian co-ordinates and V(**r**,t) is the particle/surface interaction energy. The interaction energy depends on the particle/surface system and it can be gained with trial-and-error of semi-empirical model of measurements. The initial wave functions – that are used in TEAS calculations – are Gaussian type wave packets:

$$\Psi(x,y,z,t=0) = C\,\exp(-(x-x_0)^2/2\sigma_1^{\,2} - (y-y_0)^2/2\sigma_2^{\,2} - (z-z_0)^2/2\sigma_3^{\,2})\,\exp(\mathrm{i}\,\mathbf{kr}). \tag{2}$$

Ψ is the wave function, t is the time, C is the normalisation constant, (x_0, y_0, z_0) is the average position at $t=0$, σ is the standard deviation, „*i*" is the imaginary unit, **k** is the wave number vector and **r** is the position vector. The y co-ordinate is omitted in two-dimensional calculations, namely the solid surface is only corrugated in one-dimension.

5.2 He diffraction and transfer width

Stern, Estermann and Frish demonstrated the wave theory of probe particles, when first they observed diffraction patterns of He atom and H_2 scattering from LiF and NaCl surfaces [79-81]. Varga made a computer simulation of the diffraction pattern in the case of He-W(112) model surface scattering and analyzed the transfer width as a function of energy spread of incoming atomic beam and of lattice constant [82]. To describe the interaction potential of He-W(112), a 1D corrugated Lennard-Jones-Devonshire type potential has been chosen:

$$V(x,z) = D\exp(-2\alpha z)\left\{1-2\beta\left[\cos\left(\frac{2\pi}{a}x\right)\right]\right\}. \tag{3}$$

D is the energy constant, α is the repulsive constant, β is the corrugation constant and „*a*" is the lattice constant. The standard deviation of the incoming wave packet and the period of the surface are changed and the diffraction pattern is computed and visualised. The main data of the 2D computations are the following (in atomic units (a.u.)): in eq. (2): $k_x = 0,\ k_z = -4$, in eq. (3): D=0.00012, α=0.582, β=0.2. The ground of the model calculations is the result that the energy spread is the inverse ratio to the co-ordinate spread [82]. Figure 1 shows the different stages of the

probability density functions (PDF) of the scattering in the momentum space when (in a.u.): $\sigma_1 = \sqrt{5}, \sigma_3 = \sqrt{5}$ and a=5.18. Figure 1A and figure 1I correspond to the atomic source region and the detector region, respectively. Approximately monoenergetic beam can be seen in figure 1A and clear-cut diffraction peaks are rendered in figure 1I. PDF of the interaction process is demonstrated by Figures 1B-H as a function of time.

If the transfer width is greater than the typical size of the surface period diffraction peaks are appeared. Two types of model computations are executed to analyse the connection between the transfer width and the diffraction pattern. Figure 2 shows the case when the period of the surface is constant and the energy spread of the beam is changed, namely, in the order of A, B, C and D the monochromaticity of the atomic beam is decreased. The relative velocity spread of initial wave function has been determined by Heisenberg inequality. In figure 2A and 2B there are narrow diffraction pattern, which correspond to the supersonic atomic source. There are greater FWHMs of diffraction peaks in figure 2C. Figure 2D does not show a structured intensity distribution because the transfer width is less than the period of the surface.

Let us see Figure 3. The period of the surface is changed and the energy spread of the beam is constant. In figure 3A the diffraction peaks are well defined and clear-cut peaks of the intensity distribution disappear as the lattice constant of the surface is increased significantly. The diffraction peaks overlap each other in figure 3B and 3C. The resolution of TEAS is abruptly decreased as the lattice constant is increased. In figure 3D only the specular peak can be seen and it is a narrower peak than in figure 3C.

The above results support the idea that the transfer width has to be significantly greater than the surface period. Otherwise, the resolution of the experiment is not fine enough to determine the exact surface structure.

5.3 He diffraction from clean and stepped surface

The He scattering from clean and stepped surface was investigated in the case of a general model surface and Rh(311) surface by Varga [78]. The irregularly stepped surface deforms the intensity distribution compared to the periodic surface. The deformation characterizes the surface topography. The systematic classification of model computations might provide connection to the surface structure and the intensity distribution of TEAS. Now, let us see two 3D model calculations and animations of He scattering.

First of all He scattering on Rh(311) is considered. A corrugated Morse interaction potential describes the Rh(311) surface:

$$V(\mathbf{R},z)=D\,[\,\exp(-2\alpha(z-\zeta(\mathbf{R})-disorder(x,y)))-2\exp(-\alpha(z-\zeta(\mathbf{R})-disorder(x,y)))\,], \quad (4)$$

where $\zeta(\mathbf{R})$ is the corrugation function and the position vector $\mathbf{R}$ is parallel to the surface [83]. Approximately 63 meV He beam scattered on regularly stepped Rh(311) surfaces [84]. As is known the ordered Rh(311) surface is a regularly stepped surface. Input data (a.u.) in eq. (2) are: $x_0 = 9.86, \mathrm{y}_0 = 16.84, \mathrm{z}_0 \approx 17, \quad \sigma_1 = \sigma_2 = \sigma_3 = \sqrt{5},$

$k_x = 0, k_y = 4.123, k_z = -4.123$. Input data in eq. (4) are: *D*=7.74 meV, α=1.01 1/Å, *disorder(x,y)=0* and the parameters of the corrugation function have been chosen from the literature [83]. The corrugation parameters have been fitted to the experimental results by the hard corrugated wall model. Obviously, eq. (4) does not provide the effective corrugation function. However, it is a good approach of the interaction potential in first order. The incident angle of He beam corresponds to 45°. The snapshots of PDF in the real space are rendered as a function of time with *isosurface technique*. The isosurface value is approximately 5% to the maximum of PDF at the source region. An isosurface of the interaction potential is also shown to imagine the penetration of the wave packet into the very top layer of the surface. At the initial state the isosurface is a sphere (Figure 4A) because of the input data but at the detector region a set of diffraction states is evolved containing separate domains (Figure 4I). The intermediate states inform you on the scattering dynamics. The interaction is strong in a small region near the surface.

Second example describes the interaction process near the surface – in the quantum mechanical region - *by window technique* applying a clean model surface. Lennard-Jones-Devonshire type interaction potential has been chosen [78]:

$$V(x,y,z) = D\exp(-2\alpha(z - disorder(x,y)))\left\{1 - 2\beta\left[\cos\left(\frac{2\pi}{a}x\right) + \cos\left(\frac{2\pi}{a}y\right)\right]\right\} \quad , \qquad (5)$$

where *D* is the energy constant, α is the repulsive constant, β is the corrugation constant and „*a*" is the lattice constant, *disorder(x,y)* ensures the surface disorder.

A completely periodical solid surface was analysed in the case of approximately 30 meV He beam. (Input data (a.u.) in eq. (2) are: $x_0 = y_0 = 18.13,\ z_0 = 16.67,\quad \sigma_1 = \sigma_2 = \sigma_3 = \sqrt{5},\ k_x = k_y = 0,\ k_z = -4$, input data (a.u.) in eq. (5) are: *D*=0.00012, α=0.582, β=0.2, *a*=5.18, *disorder(x,y)=0*) As is known the scattering process leads to diffractive intensity distribution. Relevant question is what happens near the surface in the quantum region. To answer this problem parallel slices of the PDF of the scattered He atoms to the solid surface have been rendered as the time propagated near the classical turning point. PDF can be obtained as a square of the absolute value of the wave function, which wave function is calculated by TDWP method. In figure 5 one can see colour scale snapshots of PDF in the momentum space as a function of time. First the wave packet is approaching to the surface, to the window parallel to the surface, where we render the slices of the PDF. Figure 5A only shows small and dim spot. The wave packet, however, is going to the surface and the window slice of PDF becomes larger and more complicated. The bright spots correspond to the diffraction channel. In the interaction region the close channels are also appeared, which evanesce during the scattering. E.g. in figure 5F and 5G one can see the two-dimensional Brillouin zones in order of first, second and third relating to a square lattice. After the interaction, the wave packet leaves behind the surface and the window slice becomes dim and empty again (Figure 5I).

Further effect is the step-edge orientation, which should be discussed by TDWP method. Helium atom scattering has been applied to determine the step-edge orientation on a Rh(311) surface, whose close-packed rows are separated by altern (100) and (111) microfacets [85]. Additional peaks were observed from the specular beam when the incident

He beam was impinging on the microfacets on the (100) or (111) microfacets. The stepped surfaces structure can be investigated by this effect.

An another new problem occurred exposing the He beam at grazing angle. Diffraction beams from the scattering of He atoms from the Rh(311) surface were observed at scattering angles of up to grazing exit at 90° with respect to the surface normal [86]. Under grazing exit conditions, a broad scattered signal appears which is interpreted as diffuse scattering of the grazing diffraction beam arising from collisions with the low density step defects resulting from the small miscut of the crystal. This experiment opens new possibilities for the characterization of surface defects with diffraction techniques. However, in the "upstairs" and "downstairs" direction there is significant difference between the intensity in (01) direction. This phenomenon is not explained by close coupling calculation but by Fraunhoffer diffraction model. The TDWP method is able to determine which direction is uphill. TDWP method, however, demands a long region parallel to the surface in the azimuth angle direction as well as absorbing boundary because of the grazing-angle.

5.4 He scattering on adsorbed surfaces

TEAS is able to determine the surface topography exploiting the intensity distribution. The diffraction beam becomes very clear-cut when the surface structure is periodic again. Exposing the surface top layer by adsorbate beam, periodic super lattice could be developed as a function of adsorbate coverage rate and of the adsorbent structure. The details of this topic are reviewed in [11]. However, let us see some experiments since these are necessary for the further discussion and provide experimental results to the theoretical TDWP calculations.

The (311) surfaces of fcc materials are of special interest as they offer a large variety of differently co-ordinated adsorption sites [87]. Rh(311) was achieved by He diffraction. Development of hydrogen phases on Rh(311) was executed by hydrogen exposure. The sequence of the superstructures in order of exposure are the following: c(1x1)H, c(1x3), p(1x1)H and p(1x1)H (REC).

The adsorption of oxygen on Rh(311) has been investigated by means of He scattering [88]. The formation of ordered (2x1) and (1x3) structures was observed. The experimental results suggest that oxygen induces a surface reconstruction in the (1x3) phase, whereby at least one of the three close-packed rows is missing and the oxygen atoms fill resulting deep troughs.

The formation of ordered structures of hydrogen on Pd(311) has been investigated with low-temperature He beams [89]. Before completion of a saturated c(1x1) phase, formation of three low-coverage (2x1) phases could be found. Possible structural models for the reported phases has also been discussed [89].

The formation of ordered oxygen overlayers on Pd(311) as well as structures obtained after their reduction in hydrogen have been studied by He scattering [90]. The presence of a pronounced rainbow pattern in the (1x2) in-plane spectra shows unambiguously that its structure is of missing-row type. Possible structural models for different phases are recommended.

Low energy vibrations of CO adsorbed on Ni(110) was investigated with high resolution He atom scattering carefully [139].

The above and other experiments were discussed in detail [11] but further investigation with TDWP method might provide additional elaboration of intensity distribution, as it is seen below.

The helium atom scattering is suitable to characterise the correct orientation in the (1x1) CO commensurate monolayer adsorbed on a single crystal NaCl(100) surface has been investigated [91]. The fully quantum mechanical description is based on two potentials which exhibit a significant discrepancy according to whether the CO axis is normal to the surface or inclined to about 40° approximately. The computation resulted that the He diffraction is suitable to determine structure of (1x1) CO phase. The TDWP method used to compute the diffraction spectra was the same as in Lemoine's paper [92] apart from a special splitting algorithm [93] . The wave function of scattering is expanded in terms of plane waves for the two-dimensional reciprocal space. In the case of off-normal He incidence the diffractive scattering symmetry was exploited [92]. The computed intensity distributions of two different CO phase positions show significant discrepancy. In the wave packet picture the trapped portion is slowly leaking out of the interaction to the asymptotic region. Even if one finally turns the grid as the wave function spreads the multidimensional computation may be too large. This problem can be resolved by complex absorbing potential or splitting the outgoing packets into an interaction piece and an asymptotic piece [93] . This splitting procedure should be repeated until the intensity of the wave function becomes negligible in the interaction region. Both the interaction and asymptotic pieces have to be back-transformed to momentum space, either for the propagation step or for the final asymptotic analyses. The splitting operator method has to avoid the discontinuities.

A numerically exact TDWP quantum calculation of the He scattering from single CO adsorbates on Pt(111) has shown that is based on a soft potential closely approximating hemisphere geometry [94]. The model calculations showed good agreement with experimental angular distribution.

5.5 He resonant adsorption on Rh(311) surface

On the basis of TDWP method calculation and assuming an exponential decay law for the resonances, Hernandez and co-workers [95] have computed the selective-adsorption resonances in the elastic scattering of He atoms from the Cu(110) and Cu(117) surfaces.

Miret-Artés [96] proposed a systematic classification of the elementary processes within the close-coupling formalism. The "term" elementary means that the entrance scattering channel directly leads to the formation of the resonance without intermediate states and the single phonon approximation holds. Fourteen different cases are discussed. There are also theoretically predicted and experimentally observed mechanisms. The multiphonon contributions to the elastic diffracted intensities and resonance profiles are considered in [97] for scattering of He atoms from surfaces Cu(110) and Cu(113).

Diffraction studies have been performed with He and Ne beams on clean Rh(311) and c(1x1)H phase [83]. Selective adsorption of He on clean Rh(311) and c(1x1)H phase could be measured, allowing the determination of three and four bound-state levels, respectively. These parameters were fitted to a two-parameter Morse potential.

Let us investigate the resonant adsorption of He-Rh(311) system with TDWP method [111]. This system is the same as it is in section 5.3 and the numerical procedure is similar to applied one. In eq. (2) the main input parameters of the He beam are (in a.u.): σ=√5, x_0=9.8644, y_0=12.681, z_0=11 and **k**=($k_x = 0$, $k_y = 3.0636$, $k_z = -2.1452$), k=3.74. The average energy of the He atom is: ≈26 meV. The incident angle is: $\Theta_i = 55^\circ$. Sample points 32, 96 and 64 are chosen in the direction *x*, *y* and *z*, respectively. In Fig. 6A and 6B the PDFs are shown in the real and in the momentum space, respectively as the wave packet is approaching the classical turning point ($< z >= 2.62$ a.u., '<>' stands for the average). PDF is equal to $|\Psi(\mathbf{r},t)|^2$. PDF is split into slices parallel to the solid surface since PDF is a function of three variables in space. In this region the He-surface interaction is essential. One can see a very important fact, for |**k**|>3.74 a.u. the probability significantly differs from zero. This corresponds to the bound states, because the perpendicular motion is limited so a fraction of the He atoms have longer life time near the Rh(311) surface. Fig. 6C and 6D show PDF after the scattering, beyond the interaction region in the real and in the momentum space. One can also see in-plane and out-of-plane scattering. The component of the wave number vector **k** parallel to the surface is shorter than 3.74 a.u. on the contrary when the He atom is near the top layer of the Rh(311) surface. The attractive part of the interaction potential leads to longer lifetime near the surface.

5.6 Classical and quantum chaos

Recently some classical and semiclassical calculations of atom scattering showed chaotic effects. Guantes at al. [98] discovered classical chaos of the He scattering on Cu(117) relating to the right angle rainbow scattering. The scattering phenomenon becomes extremely sensitive of the scattering parameter. This fact yields the fractal structure of the curve of the He atom deflection angle - impact parameter [99].

Miret-Artés at al. showed that the diffraction condition for the scattering of atoms from surfaces leads to the appearance of a distinct type of classical singularity [100]. It is also shown that the onset of classical trapping and chaos is closely related to the bifurcation-order function around the surface points showing the rainbow effect. The scattering of He atoms on stepped Cu(115) is discussed.

Guantes and his co-workers [101] investigated the phase diagrams (e.g. periodic orbits and homoclinic tangle) of He atom scattering on Cu surface considering the chaotic scattering within the frame of the classical theory.

A classical picture of threshold resonances in classical chaotic-surface scattering is explored [102]. It is also emphasized that these resonances are observable for highly corrugated surfaces or for smooth surfaces with incident conditions where multiple scattering is important.

The semiclassical S-matrix theory is applied in the case of classically chaotic scattering [103]. According to the basic assumption the direct and complex contributions to the S matrix can be computed independently. Only the interference among trajectories corresponding to the same "icicle" is considered. If a chattering region (irregular

curve) is expanded, a series of smooth subdomains – called "icicles" – can be found. This is equivalent to assume the interferences between all trajectories in different icicles will cancel each other on average.
Hernández et. al. [104] investigated the time evolution of He scattering on Cu(110) by time dependent autocorrelation function of a wave packet. Wave packet time propagation was determined by solving the TDSE using a finite difference scheme. All the memory of the initial wave packet was rapidly lost. The same results were received by a method of half-width analysis.

Classical models of scattering techniques often show chaotic behaviour. This fact induces the question of quantum chaos. Intensities of low energy electron diffraction and photoelectron diffraction are analyzed from a statistical point of view in [105]. To characterize chaotic wave functions Porter and Thomas advanced the hypothesis that *wave functions of a chaotic system should display a* χ_ν^2 *statistical probability distribution* [106]. This hypothesis has been rigorously justified by the supersymmetry formalism [107], and has been used as a convenient definition of quantum chaos. This hypothesis at least can be thought as a necessary condition. Dyson [108] demonstrated that within the random matrix theory [109] only three universal classes exist. Depending on whether the Hamilton operator is constructed with real numbers, complex numbers or quaternions, ν is 1, 2 or 4 degrees of freedom, respectively.
A good understanding of wave functions is crucial in explaining open systems, namely the probe-target-probe setup that is used in most scattering arrangements. In the case of quantum scattering phenomena ν degrees of freedom is 2, because the wave functions are complex functions. The calculations by Andres and Vergés [105][110] proved that the intensity distribution of the low-energy electron diffraction (LEED) and the photoelectron diffraction (PED) fit quite well to the χ_2^2 statistical distribution. The most complex models of LEED and PED fit to the χ_2^2 statistical distribution the best. These systems exhibit quantum chaos in the case of scattering on ordered surfaces, which is a remarkable result.

5.6.1 Manifestation of Quantum Chaos in TEAS

Present author was inspired to investigate the quantum chaos of TEAS on the basis of section 5.6. Recently, Balázs at al. discovered chaotic effect of the three-dimensional He-Rh(311) sytem [111]. However, the searching for quantum chaos was unsuccessful. The dwell time of the He atom - in a chosen volume - was the physical quantity that should have shown stochastic behaviour. Now, we analyzed the diffraction pattern of He-W(112) model surface [82] at the detector region. The PDF has been determined by TDWP method for the absolutely same system that was shown in section 5.2 and in Figure 1. Figure 7 shows a quite good agreement between the calculated scattering cumulative probability function of the PDF and the χ_2^2 law. *This preliminary result manifests the quantum chaos of He-W(112) model surface scattering albeit that a well ordered system was dissected.* This corresponds to the quantum chaotic behaviour of LEED and PED. The elaboration of the quantum chaos in case of TEAS will be published elsewhere.

5.7 Scattering from vibrating surfaces

A very detailed review can be found in [12] devoted to single- and multiphonon processes of TEAS. The projectile particle colliding with a surface may exchange zero, one or more quanta with the phonon heat bath. Consequently there is nonzero probability of elastic scattering; this circumstance demands scattering boundary conditions on perturbing potential of phonon processes [112]. Under certain conditions the motion of probe particles and surface vibrations can be treated by classical mechanics. This is likely to be the case for large mass of probe particle and surface atoms and high projectile incident energy [113]. Several various semiclassical schemes and approximations have been developed. For example the probe particle translational degrees of freedom are treated classically or semiclassically (heavy probe particles) and surface vibrational degrees of freedom quantum mechanically. In another case the light probe particle is treated within quantum mechanics and surface degrees of freedom classically. The classical treatment of surface vibrations is usually described by the generalized Langevin equation [114]. A quantum treatment of light atom-surface inelastic scattering proves indispensable under scattering conditions typical of TEAS [115-116]. Standard quantum mechanical theory of scattering is well-established [117-118]. The applicability of the previously mentioned approaches depends on the scattering regime (classical, semiclassical or quantum) in which the experiments have been carried out. An unified theory of He scattering of thermal energy should contain the quantum formalism, unitarity in the sum of all scattering probabilities, full surface vibrational dynamics, limit in the one-phonon scattering regime and quantum treatment of multiphonon scattering in three dimensions. The scattering spectrum approach model (SSA) wants to fulfil the conditions of unification [119]. Different developments can be found in [120-123] - the calculations of Debye-Waller factors, Born approximations, or He energy transfer to surfaces.

One can see how complicated is the question of the coupling between the probe particle and solid surface. The advantage of TDWP is that the surface may contain arbitrary disorders and the atomic beam may be non-monoenergetic. The disadvantage of TDWP is the limited number of the degree of freedom in consequence of high computer effort. If one wants to exploit the quantum description of TDWP then three degrees of freedom are occupied for translational motion of probe atom. A classical coupling can be provided with classical discussion of solid surface vibration via the generalized Langevin equation [114]. The surface consists of two zones. In the first zone there are the target atoms, which directly collide with probe atoms. The second zone contains the surface atoms, which experiences the interaction with probe atom described via the so-called memory function. This model should contain ordinary coupled differential equations of surface atoms. These equations are related to the time dependent Schrödinger equation and vice versa. The coupling is attained via the interaction energy between the scattering atom and the pair-wise surface potential. If the scattering atom does not influence the surface atoms; the approximation corresponds to pure thermally vibrating system without energy change. This is the simple kinematic theory [70]. TDWP method with Langevin equation will be published elsewhere in details.

6. Molecule scattering on solid surfaces

A fruitful application of TDWP method is the investigation of reactions at surfaces [124-125]. Understanding reactions on surfaces plays an important role in heterogeneous catalysis, crystal growth determining the quality of semiconductor devices; corrosion and lubrication, influencing the durability of mechanical systems; or hydrogen storage in metals and so on. In the last decade the increase of the computer power and the development of ab initio surface calculation led to the fully quantum mechanical dynamic calculation of scattering of diatomic molecules (mainly H_2) from solid surfaces. So-called ab initio dynamics calculations of reactions on surfaces usually require three independent steps:

- determination of ab initio potential energy surface (PES) by first-principle total-energy calculations,
- a fit of the total energies to an analytical or numerical continuous representation which serves as an interpolation between the actually calculated points,
- a dynamical calculation on this representation of the ab initio PES that includes all relevant degrees of freedom.

6.1 Theoretical background of molecule/surface dynamics

To take into account a fully quantum mechanical calculations to analyse the dynamics of molecule surface interaction some relevant theoretical approximations are necessary. Detailed description can be found in [125-126]. Based on the papers [125-126] a short description of molecule-surface dynamics can be read below.

One common approach is to assume that – due to the large mass difference between electrons and the nucleus – the electrons follow the motion the nucleus adiabatically. This is the *Born-Oppenheimer approximation* [127]. In gas-surface scattering electronically non-adiabatic processes are indeed occurring. However, the proper treatment of non-adiabatic processes is rather complex. To solve the Schrödinger equation here is too complex since the phonons have infinite degrees of freedom.

The additional approximation consists of surface atoms frozen to their ideal lattice positions, thereby *neglecting the phonons*. This model can be handled fully quantum mechanically in the case of diatomic molecules as we discuss it below. The reaction probability curve is characterized by three parameters: the maximum reaction probability, the width parameter and the dynamical barrier height. The mere presence of phonons at zero surface temperature may have an effect on computed reaction probability, which can only be assessed in theoretical calculations. The reaction probability may be affected by alterations in surface temperature in experiments as well as calculations. In several cases, the maximum probability and the dynamical barrier height are independent of surface temperature. This fact means the frozen surface approximation determines the dynamical height barrier within a few hundredths of an eV. The effect of surface temperature may be taken into account by readjusting the width parameter of the reaction

probability curve to the surface temperature. For non-activated reactions, the reaction probability is always large, and we would expect the surface temperature to be even less important for these reactions.

The calculation of potential energy surface is based on *density functional theory* (DFT) [128-129]. One serious problem arises for the use of ab initio potential energies in particular in quantum dynamics simulations. To solve the Schrödinger equation, one needs in general a continuous description of the potential since the wave functions are delocalized. The ab initio calculations provide total energies for discrete configurations of the nuclei. In order to obtain a continuous description, the ab initio energies have to be fitted to an analytical or numerical continuous representation of the potential energy surface.

At last the Hamilton operator of the diatomic molecular beam scattering on a rigid solid surface is:

$$H_{6-D} = -\frac{\hbar^2}{2M}\nabla^2_{\mathbf{R}} - \frac{\hbar^2}{2m}\nabla^2_{\mathbf{r}} + V_{6-D}(\mathbf{R},\mathbf{r}),$$

where $\mathbf{R}(x,y,z)$ is the vector of molecule center-of-mass. (x,y) is parallel and z perpendicular to the surface. M is the molecule mass and m is the reduced mass of the molecule ($m = (m_1 m_2 / (m_1 + m_2))$). Furthermore, $\mathbf{r}$ is the vector of the internal co-ordinates of the molecule, which are usually taken as (r, Θ, Φ). r is the distance of atoms of the molecule, Θ is the polar and Φ is the azimuthal angle of orientation of the molecular axis.

We have two basic different ways to determine the wave function. The first way is the solution of time independent Schrödinger equation (TISE); the second one is the solution of time dependent Schrödinger equation (TDSE). The 6D dynamical problem have been formulated using coupled channel (CC) method, i.e., by writing TISE as a set of coupled ordinary differential equations instead of partial differential equation in a scattering co-ordinate system [126]. The goal is to obtain the scattering S-matrix by coupled channel method, which corresponds to the elastic or the inelastic scattering. Since the potential energy surface is conservative, the total energy of the probe particle is constant during the whole process. However, there are open channels between the different states, e.g., the vibrational and the rotational states. The vibrational or the rotational energy may change and we speak - in this sense - about the inelastic scattering. The solution of TDSE by TDWP method is discussed in previous sections. For problems involving small scattering basis sets, the computational effort of the CC method may be comparable with the computational effort of the TDWP method [130-131]. However, involving bigger scattering basis set the TDWP calculations becomes less expensive. The TDWP method will be the most efficient, if the goal is to obtain results for one initial state, but for a large range of energies. CC method demands much smaller computer memory than TDWP method.

Typical quantum numbers are the following: reciprocal lattice vector co-ordinates (m,n), the diffraction quantum numbers; vibrational quantum numbers (v); rotational (angular) quantum numbers (j) and magnetic rotational quantum numbers (m_j). Diffraction quantum numbers refer to periodic solid surface. It is worth describing the

rotational state $\left| jm_j \right\rangle$ by spherical harmonic functions and the vibration by rovibrational state $\left| \nu\ j \right\rangle$. The effect of alignment (m_j) on reaction is important, particularly two special positions: the $m_j = 0$ "cartwheel" state and the $m_j = j$ "helicopter" state. Cartwheel state rotates in a plane perpendicular to the surface, helicopter in a plane which is approximately parallel to the surface, m_j being the projection of *j* on the surface normal.

Investigating the molecule scattering by above described model, the diffraction probability and the sticking probability can be computed, too. The sticking may yield dissociative adsorption. The final states show an appropriate distribution of possible quantum states. This means the evolution of different rovibrational, rotational and translational final states. The experiments and theoretical calculations led to better understanding the molecule/surface dynamics. For example, the *steering effect* was underestimated hitherto. A qualitative explanation of the steering effect is the following. Let us imagine a classical trajectory model and let the molecule position be perpendicular to the surface at perpendicular incident angle. At the initial state, the molecule can be found in a plane that is perpendicular to the surface. This is a special type of cartwheel position. If the initial kinetic energy is low enough, then the molecule has enough dwell time to be reoriented approximately parallel to the surface. This position means a much higher probability of dissociative adsorption. If the kinetic energy is high enough, the molecule is so fast that it hits the repulsive wall of the potential before it is in a favourable configuration to dissiciative adsorption. The molecule is scattered back into the gas phase rotationally excited.

6.2 Applications of molecular beam scattering

At last, we mention some results of TDWP, CC methods and experiments concerning molecule/surface dynamics. Molecular beam experiments have simultaneously measured not only the diffraction peaks but the rotational state of H_2 scattered from the surface, and observed rotationally inelastic diffraction, e.g., Ag(111) (ref. [132]), Rh(110) (ref. [133]), Ni(110) (ref. [134]), Cu(001) (ref. [135-136]), LiFl(001) (ref. [137-138]). Elastic rotationally mediated critical kinematic selective adsorption (RMCK-SA) is experimented in the scattering of D molecule from the Cu(001) surface [140-141]. In a series of diffraction spectra taken for different surfaces temperatures between 40 and 500 K resonance lineshapes are observed. The RMCK-SA effect results from the interaction among several diffraction and rotational channels. From the best fit of the experimental profiles a lifetime for the third bound state of the D molecule-Cu interaction potential is obtained.

Dai and Light [142] presented a six dimensional quantum wave packet dynamics calculation for dissociative adsorption of H molecule on Cu(111) surface. The energy surface was taken into account by ab initio calculations [143]. The dissociation probability with different quantum number was determined for all degrees of freedom: namely the three Cartesian co-ordinates of the centre of mass and three internal co-ordinates.

Diño et al. investigated the dissociative adsorption dynamics of D molecule on Cu(111) surface using the coupled channel method [144]. To explain experimental observations, it is necessary to consider the coupling between the rotational degree of freedom of the impinging molecule and the vibrational degree of freedom of the surface.

Harris and co-workers [145] compared a mixed quantum-classical treatment of molecule-surface scattering and dissociation dynamics with classical and exact quantum methods. They found that the accuracy of the semi-quantal method is at best as good as the classical, while the computational performance is considerably poorer.

The quantum dynamics have been solved by wave packet techniques in the case of H_2 scattering [146-147]. To prevent reflections from the ends of the grid, grid-cutting techniques have been used [93][148].

McCormack and Kroes [149] executed a direct comparison between classical/quasiclassical trajectory results and the six-dimensional quantum wave packet method in case of adsorption of H molecule on Cu(100) surface. The quasi-classical reaction probability is in much better agreement with the quantum probability than the classical.

Hydrogen molecule adsorption on Pd(100) is determined in [150] by ab initio quantum and coupled channel molecular dynamics calculations. It is shown that the determination of the potential-energy surface combined with high-dimensional dynamical calculations leads to a thorough understanding of the hydrogen dissociation dynamics at a transition metal surface. All relevant degrees of freedom are taken into account.

Miura et al. [151] investigated how the coupling between molecular vibration and rotation affects the direct scattering of H_2 from Cu(111) by performing coupled channel computations. The conclusion is that the rotational excitation in vibrationally elastic scattering processes occur more preferentially for H_2 in vibrational excited state than for H_2 in vibrational ground state in low translational energy region, because the decrease of vibrational energy in transition state region is larger for excited state than for ground state.

How orientation influences H_2 dissociative dynamics at different sites along the $Cu_3Pt(111)$ surface lateral direction where Cu and Pt alternate is studied in [152]. Computational results show a strong dependence of H_2 dissociation on the H_2 orientation across Cu-Pt bridge site.

Miura at al. [153] inquired into the isotope effect on rotationally inelastic diffraction dynamics of hydrogen scattered from Cu(001) executing coupled channel calculations. Strong isotope effect has been observed, viz., in the low incident energy region, the rotationally inelastic diffraction probabilities of D molecule are larger than those of H molecule. Increasing incident energies, however, the rotationally inelastic diffraction probabilities become smaller than in the case of H molecule.

Miura and co-workers [154] investigated the effect of the correlation between molecular diffraction and rotational excitation on the scattering dynamics of H_2 scattering from Cu(001). Apart from some oscillatory structures, rotationally probabilities show opposite incident energy dependence for H_2 doing cartwheel-like rotations (increase with increasing incident energies) and helicopter-like rotations (decrease with increasing incident energies).

A time dependent quantum mechanical study of the *chemisorption* dynamics of H_2 scattering on W(001) is presented in [155]. Bejan and co-workers [156] have investigated the *desorption* of CO on Cu surfaces that is

induced by hot electrons. The results of the wave packet computations are in fair agreement with the experimental findings.

Eley-Rideal (ER) reactions are investigated between H atoms on metal and graphite surfaces [157]. In ER reaction, a gas-phase particle incident on a substrate combines with a particle adsorbed onto that substrate contrary to a Langmuir-Hinshelwood reaction involving diffusing reactant atoms. In general, the TDWP method of the Eley-Rideal reactive scattering between a gas phase atom and an adsorbate is discussed in [158]. This paper contains the description of a computer program that handles the ER problem solving TDWP method in three-dimension.

Six-dimensional quantum and classical dynamics computations of H_2 scattering on Pt(111) are presented [159]. The quantum calculation results are in good agreement with recent molecular beam experiments. Quasi-classical method works better than classical method, the quasi-classical results being in excellent agreement with the quantum results. The physical model consists of Born-Oppenheimer approximation and the reaction takes place on the ground state potential energy surface. The Pt surface is frozen, Pt atoms are in equilibrium positions. The remained six degrees of freedom is treated without further physical approximation. The most expensive calculation contains 168.5 million grid points in the six-dimensional discretized physical space. This quantum computation is a typical TDWP method.

The feasibility of utilizing hydrogen molecules to probe adsorbate-surface interaction, the surface structure, and the effective potential energy surface to the reaction considered are explored in [160]. Based on the calculations and according to the experiments with $H_2/Cu_3Pt(111)[1\bar{2}1]$, $H_2/NiAl(110)[1\bar{1}0]$, $H_2/Cu(001)[100]$ the scattering of H_2 is able to distinguish among various components on surfaces.

7. Conclusions

Time dependent wave packet method has been reviewed emphasising its recent applications, numerical solutions and computer animation techniques. Reactive scattering of atom and molecules, atomic and nuclear phenomena in laser fields, electron scattering from molecule, photodissociation, photoabsorption, nonadiabatic processes of molecules, Rutherford scattering, electrons in nano-scale devices, cooling and trapping in quantum wires and dots, scanning tunneling microscopy, thermal energy atomic scattering and molecular beam scattering are the recent applications to TDWP method, which are involved at present work especially focusing on TEAS and MBS. Among other things quantum chaotic behaviour of TEAS from an ordered surface has been demonstrated first. The long list of applications supports the importance of TDWP method. The relevance of TDWP method eventuates the progression of the numerical procedures and the simulation methods (e.g. animation techniques). The animation techniques might lead to more accurate understanding of physical processes. The further researches might discuss more complicated atom/molecule – surface interactions: e.g. recording step-edge orientation by TEAS; grazing angle TEAS; quantum chaos of TEAS from ordered and disordered surfaces and molecular dynamics of polyatomic molecules relating to frozen or vibrating surfaces.

Appendix

It is shown the determination of some physical quantities from the wave function without completeness. The notation system is the following: Ψ is the state function, **r** is the position vector, *t* is the time, *F* is the operator of a physical quantity, **k** is the momentum vector, *m* is the particle mass, **„***i*" is the imaginary unit and „*' is the conjugate.

Average of a physical quantity is $\int_V \Psi^*(\mathbf{r},t)\, F\, \Psi(\mathbf{r},t) dV$, *V* is the whole space.

Probability density function in real space is $PDFR = \Psi^*(\mathbf{r},t)\Psi(\mathbf{r},t)$.

Probability density function in momentum space is $PDFM = \tilde{\Psi}^*(\mathbf{k},t)\tilde{\Psi}(\mathbf{k},t)$.

Probability current density: $\mathbf{j} = \frac{\hbar}{2mi}\left[\Psi(\mathbf{r},t)^* \nabla\Psi(\mathbf{r},t) - \left(\nabla\Psi(\mathbf{r},t)^*\right)\Psi(\mathbf{r},t)\right]$.

Probability current to a surface: $I = \int_A \mathbf{j}\, d\mathbf{A}$.

Dwell time probability $P(t) = \int_{t_0}^{t}\int_{V_0} \left|\Psi(\mathbf{r},t)\right|^2 dVdt$ t_0 is the time when the measurement is started, and $t \geq t_0$ is the measurement time. V_0 is the investigated volume. *P*(*t*) is a fraction of $(t - t_0)$ [111].

Dwell time probability density is $\int_{t_0}^{t} \left|\Psi(\mathbf{r},t)\right|^2 dt$.

The time independent wave function of Schrödinger equation is $\psi(\mathbf{r},E) = \frac{1}{2\pi}\int_{-\infty}^{\infty} \exp(iEt)\Psi(\mathbf{r},t)dt$ (time-to-energy Fourier transformation).

References

[1] N. García, J. Chem. Phys. 67 (1977) p. 897.

[2] E. Stoll, M. Baumberger and N. García, J. Chem. Phys. 81 (1984) 1496.

[3] L. Füstöss and G. Varga, Vacuum 40 (1990) pp. 47-50.

[4] G. Varga and L. Füstöss, Vacuum 41 (1990) pp. 315-317.

[5] G. Varga and L. Füstöss, Surface Science 243 (1991) pp. 23-30.

[6] G. Varga and L. Füstöss, 1990. XI. Yugoslav Vacuum Congress, Zveza drustev za vakuumsko tehniko Jugoslavije, volume. 24 (1990) pp. 382-390.

[7] G. Varga, Vacuum 50 (1998) pp. 339.

[8] B. Salanon and G. Armand, Surf. Sci. 112 (1981) p. 78.

[9] N. Cabrera, V. Celli, F.O. Gooman and R. Manson, Surf. Sci. 19 (1970) p. 67.

[10] E. Balázs and G. Varga, Vacuum 37 (1987) pp. 153-156.

[11] D. Farías. K.H. Rieder, Rep. Prog. Phys. 61 (1998) pp. 1575-1664.

[12] B. Gumhalter, Phys. Rep. 351 (2001) pp. 1-159.

[13] S.Y. Lina, K.L. Hana and J.Z.H. Zhang, Chem. Phys. Lett., 324 (2000) pp.122-126 .

[14] R. Schinke, J. Chem. Phys. 80 (1984) p. 5510.

[15] N.J. Clarke, M. Sironi, M. Raimondi, S. Kumar, F.A. Gianturco, E. Buonomo and D.L. Cooper, Chemical Physics 233 (1998) pp. 9-27.

[16] Y.C. Zhang, Z. Tan, H. Zhang, Q. Zhang and J. Z. H. Zhang, Chemical Physics, 252 (2000) pp.191-197.

[17] D. Domenico, M.I. Hernández, and J. Campos-Martínez, Chem. Phys. Lett. 342 (2001) pp. 177-184.

[18] Y. C. Zhang, L. X. Zhan, Q. G. Zhang, W. Zhu and J. Z. H. Zhang, Chem. Phys. Lett. 300 (1999) pp. 27-32.

[19] F. Ehlotzky, Physics Reports 345 (2001) pp. 175-264.

[20] M. Ferrero and F. Robicheaux, Chemical Physics 267 (2001) pp. 93-98.

[21] Z. Shen, I. Boustani, M. Erdmann and V. Engel, Chem. Phys. Lett. 339 (2001) pp. 362-368 .

[22] G. Barinovs, N. Markovic and G. Nyman, Chem. Phys. Lett. 315 (1999) pp. 282-286.

[23] K.C. Kulander, C. Cerjan and A.E. Orel, J. Chem. Phys. 94 (1991) pp. 2571-2577.

[24] H. Zhang, Ke-Li Han, Guo-Zhong He and Nan-Quan Lou, Chem. Phys. Lett. 289 (1998) pp. 494-499.

[25] N. Balakrishnan, A. B. Alekseyev and R. J. Buenker, Chem. Phys. Lett. 341 (2001) pp. 594-600.

[26] S. Mahapatra, H. Köppel, L. S. Cederbaum, P. Stampfuß and W. Wenzel, Chemical Physics, 259 (2000) pp. 211-226 .

[27] C.J. Sweener and P.L De Vries, Computers in Physics JAN/FEB (1989) pp. 49-54.

[28] H. De Raedt, Computer Simulation of Quantum Phenomena in nano-scale devices, Annual Reviews of Computational Physics IV, (1996) pp. 107-146, ed. D. Stauffer, World Scientific 1996.

[29] H. De Raedt, Quantum Dynamics in nano-scale devices, Computational Physics, pp. 209-224, ed. K.-H. Hoffmann and Schreiber, Springer (1996).

[30] H. De Raedt and K. Michielsen, Proc. IVMC'96, Eds. D. Glazanov, (1996).

[31] E. Andersson, and S. Stenholm, Opt. Commun. 188 (2001) pp. 141-148.

[32] G.I. Márk, L.P. Biró and J. Gyulai, Phys. Rev. B 58 (1998) pp. 12645-12648.

[33] G.I. Márk, L.P. Biró, J. Gyulai, P.A. Thiry, A.A. Lucas and P. Lambin, Phys. Rev. B 62 (2000) pp. 2797-2805.
[34] G.I. Márk, L.P. Biró and P. Lambin, Modeling and interpretation of STM images of Carbon nanotubes, NATO ARW Kiev (2001) September.
[35] G.I. Márk, Home Page: http://newton.phy.bme.hu/education/schrd/index.html
[36] B. Forenberg, SIAM J. Numer. Anal. 12 (1975) pp. 509.
[37] S.A. Ország, J. Comput. Phys 37 (1980) p. 93.
[38] M.D. Feit, J.A. Fleck and A. Steiger, J. Comput. Phys. 47 (1982) pp. 412-433.
[39] D. Kosloff and R. Kosloff, J. Comput. Phys. 52 (1983) pp. 35-53.
[40] O.V. Vasilyev and S. Paulocci, J. Comput. Phys. 138 (1997) pp. 16-56.
[41] S. Sahrakorpi, Home Page: http://alpha.cc.tut.fi/~sahrakor/research/teksti/teksti.htm
[42] H. Tal-Azer and R. Kosloff, J. Chem. Phys. 81 (1984) p. 3967.
[43] D. Kosloff and H. Tal-Azer, J. Comput. Phys. 104 (1993) pp. 457-469.
[44] A. Askar and S. Cakmark, J. Chem. Phys. 68 (1978) pp. 2794-2798.
[45] M. Suzuki, J. Math. Phys. 26 (1985) pp. 601-612.
[46] M. Suzuki, Phys. Lett. A 146 (1990) pp. 319-323.
[47] M. Suzuki, J. Math. Phys. 32 (1991) pp. 400-407.
[48] A.D. Bandrouk and H. Shein, Chem. Phys. Lett. 176 (1991) pp. 428-432.
[49] A. Rouhi and J. Wright, Computers in Physics 9 (1995) pp. 554-563.
[50] C. Lánczos, J. Res. Natl. Bur. Stand. 45 (1950) pp. 255.
[51] T.J. Park and J.C. Light, J. Chem. Phys. 85 (1986) pp. 5870-5876.
[52] H. Tal-Azer, R. Kosloff and C. Cerjan, J. Comput. Phys. 100 (1992) pp. 179-187.
[53] R.B. Gerber, R Kosloff and M. Berman, Comput. Phys. Rep. 5 (1986) pp. 59-114.
[54] R. Kosloff, J. Phys. Chem. 92 (1988) pp. 2087-2100.
[55] G.D. Billing, Comput. Phys. Rep. 12 (1990) pp. 383-450.
[56] C. Leforester, R.H. Bisseling, C. Cerjan, M.D. Feit, R. Friesner, A. Guldberg, A. Hammerich, G. Jolicard, W. Karrlen, H.-D. Meyer, N. Lipkin, O. Roncero and R. Kosloff, J. Comput. Phys. 94 (1991) pp. 59-80.
[57] B. Thaller, Visual Quantum Mechanics, Springer-Verlag (2000), ISBN 0-387-98929-3.
[58] M.V. Korolkov and K.M. Weitzel, Chemical Physics 252 (2000) pp. 209-219.
[59] M.V. Korolkov and G.K. Paramonov. Phys. Rev. A 57 (1998), pp. 4998.
[60] R.N. Bisseling, R. Kosloff and J. Manz, J. Chem. Phys. 83 (1985), pp. 993.
[61] G. Dattoli, A. M. Mancho, M. Quattromini and A. Torre , Radiation Physics and Chemistry 61 (2001) pp. 99-108.
[62] J.P. Palao and J.G. Muga, Chem. Phys. Lett. 292 (1998) pp. 1-6.
[63] H. Jiang and X.S. Zhao, Chem. Phys. Lett. 319 (2000) pp. 555-562.
[64] M. Nest, U. Kleinekathöfer, M. Schreiber and P. Saalfrank, Chem. Phys. Lett. 313 (1999) pp. 665-669.
[65] T. Yu. Mikhailova and V. I. Pupyshev, Physics Letters A, 257, (1999) pp. 1-6.

[66] D.M. Gollub and D.G. Richards, Scattering of Quantum Wave Packets, Physics on Parallel Computers, Project Description, Department of Physics and Astronomy, The University of Edinburgh (1996), Home Page: http://cip.physik.uni-wuerzburg.de/~dkgollub
[67] J.L. Richardson, Computer Physics Communication 63 (1991) p. 84.
[68] G.C. Corey and D. Lemoine, J. Chem. Phys. 97 (1992) pp. 4115-4126.
[69] D. Lemoine, Computer Physics Communications 99 (1997) pp. 297-306.
[70] G. Varga, Surf. Sci. 482-485 (2001) pp. 1152-1158.
[71] G. Varga, Home Page: http://goliat.eik.bme.hu/~vargag.
[72] J. K. Burgoon, J. A. Bonito, B. Bengtsson, C. Cederberg, M. Lundeberg and L. Allspach, Computers in Human Behaviour 16 (2000) pp. 553-574.
[73] D. J. Murray-Smith, Mathematics and Computers in Simulation 53 (2000) pp. 239-247.
[74] R. Guantes, F. Borondo, C. Jaffé and S. Miret-Artés, Surf. Sci. Lett. 338 (1995) pp. L863-L868.
[75] A.S. Sanz, F. Borondo and S. Miret-Artés, Phys. Rev. B 61 (2000) pp. 7743-7751.
[76] E.J. Heller, J. Chem. Phys. 62 (1975) p. 1544.
[77] A.S. Sanz, F. Borondo and S. Miret-Artés, Europhys. Lett., 55 (2001), pp. 303–309.
[78] G. Varga, Surf. Sci. 441 (1999) p. 472.
[79] I. Estermann and O. Stern, Z. Physik 61 (1930) p. 953.
[80] I. Estermann, R. Frish and O. Stern, Z. Physik 73 (1931) p. 348.
[81] R. Frish and O. Stern, Z. Physik 84 (1933) p. 430.
[82] G. Varga, Applied Surface Science 144-145 (1999) pp. 64-68.
[83] R. Apel, D. Farías, H. Tröger, E. Kristen and K.H. Rieder, Surf. Sci. 364 (1996) pp. 303-311.
[84] B. Poelsema and G. Comsa, Scattering of Thermal Energy Atoms from Disordered Surfaces, Springer, Berlin, 1989.
[85] M. Patting, D. Farías and K.H. Rieder, Phys. Rev. B 62 (2000) pp. 2108-2112.
[86] D. Farías, M. Patting, K.-H. Rieder and J.R. Manson, Surf. Sci. Lett. 480 (2001) pp. L395-L401.
[87] R. Apel, D. Farías, H Tröger and K.H. Rieder, Surf. Sci. 331-333 (1995) pp. 57-61.
[88] D. Farías, H. Tröger and K.H. Rieder, Surf. Sci. 331-333 (1995) pp.150-155.
[89] D. Farías, H. Tröger, M. Patting and K.H. Rieder, Surf. Sci. 352-254 (1996) pp. 155-160.
[90] D. Farías, M. Patting and K.H. Rieder, Surf. Sci. 385 (1997) pp. 115-122.
[91] M.-N. Carré, D. Lemoine, S. Picaud and C. Girardet, Surf. Sci. 347 (1996) pp. 128-142.
[92] D. Lemoine, J. Chem. Phys. 101 (1994) p. 4343.
[93] R. Heathet and H. Metiu, J. Chem. Phys. 86 (1987) p. 5009.
[94] D. Lemoine, Phys. Rev. Lett. 81 (1998) pp. 461-464.
[95] M. Hernández, J. Campos-Martínez and S. Miret-Artés, Phys. Rev. B 49 (1994) p. 8300-8309.
[96] S. Miret-Artés, Surf. Sci. Lett. 366 (1996) pp. L735-L741.
[97] S. Miret-Artés, Surf. Sci. Lett. 366 (1996) pp. L681-L684
[98] R. Guantes, F. Borondo, C. Jaffé and Miret-Artés, Internatioanal. Journal of Quantum Chemistry 52 (1994) pp. 515-525.

[99] F. Borondo, C. Jaffé and Miret-Artés, Surf. Sci. 317 (1994) p. 211.

[100] S. Miret-Artés, J. Margalef-Roig, R. Guantes, F. Borondo and C. Jaffé, Phys. Rev. B 54 (1996) pp. 10397-10400.

[101] R. Guantes, Borondo and S. Miret-Artés, Phys. Rev E 56 (1997) pp. 378-389.

[102] R. Guantes, F. Borondo, J. Margalef-Roig, S. Miret-Artés and J.R. Manson, Surf. Sci. Lett. 375 (1997) pp. L379-L384.

[103] R. Guantes, F. Borondo and C. Jaffé, Phys. Rev. B 53 (1996) pp. 14117-14126.

[104] M. Hernández, S. Serna, O. Roncero, S. Miret-Artés, P. Villarreal and G. Degado-Barrio, Surf. Sci. 251/252 (1991) pp. 373-376.

[105] P.L. de Andres and J.A. Vergés, Phys. Rev. Lett. 80 (1998) pp. 980-983.

[106] C.E. Porter and R.G. Thomas, Phys. Rev. 104 (1956) p. 483.

[107] K.B. Efetov and V.N. Progodin, Phys. Rev. Lett. 70 (1993) p. 1315.

[108] F.J. Dyson, J. Math. Phys. 3 (1962) p. 140.

[109] M.L. Mehta, Random Matrices (Academic Press, San Diego, CA, 1991), 2nd ed.

[110] P.L. de Andres and J.A. Vergés, Phys. Rev. B 59 (1999) pp. 3086-3094.

[111] E. Balázs, G. Varga and L. Füstöss, Surf. Sci. 482-485 (2001) pp. 1145-1151.

[112] B. Gumhalter, K. Burke, D.C. Langreth, Surf. Rev. Lett. 1 (1994) p. 133.

[113] A. Bilic, B. Gumhalter, W. Mix, A. Golichowski, S. Tzanev and K.J. Snowdon, Surf. Sci. 307-309 (1994) p.165.

[114] R. Gerber, Chem. Rev. 87 (1987) p. 29.

[115] A. Siber, B. Gumhalter, Surf. Sci. 385 (1997) pp. 270-280.

[116] A. Siber, B. Gumhalter, Phys. Rev. Lett. 81 (1998) p. 1742.

[117] M.L. Goldberger, K.M. Watson, Collision theory, Wiley, New York, 1964.

[118] W. Brenig, R. Haag, Fort. Phys. (Berlin) VII (4/5) (1959) p. 183.

[119] A. Bilic, B. Gumhalter, Phys. Rev. B 52 (1995) p. 12307.

[120] B. Gumhalter, Prog. Surf. Sci. 15 (1984) p. 1.

[121] B. Gumhalter, D.C. Langreth, Phys. Rev. B60 (1999) p. 2789.

[122] A. Siber, B. Gumhalter and J.P. Toennis, Vacuum, 54 (1999) pp. 315-320.

[123] B. Gumhalter, Surf. Sci. 347 (1996) pp. 237-248.

[124] U. Manthe and H. Köppel, Chem. Phys. Lett. 178 (1991) pp. 36-42.

[125] A. Gross, Surf. Sci. Rep. 32 (1998) pp. 291-340.

[126] G.-J. Kroes, Prog. Surf. Sci. 60 (1999) pp. 1-85.

[127] M. Born and J.R. Oppenheimer, Ann. Phys. 84 (1927) p.457.

[128] R.M. Dreizler E.K.U. Gross, Density Functional theory, Springer, Berlin 1990.

[129] M.C. Payne, M.P. Teter, D.C. Allan, T.A. Arias and J.D. Joannopoulos, Rev. Modern Phys. 64 (1992) p. 1045.

[130] G.J. Kroes, R.C. Mowrey, J. Chem. Phys. 101 (1994) p. 805.

[131] R.C. Mowrey, G.J. Kroes, J. Chem. Phys. 103 (1995) p.1216.

[132] K.B. Whaley, C. Yu, C.S. Hogg, J.C. Light and S.J. Sibener, J. Chem. Phys. 83 (1985) p. 4235.

[133] D. Cvetko, A. Morgante, A. Santaniello and F. Tommasini, J. Chem. Phys. 104 (1996) p. 7778.
[134] M.F. Bertino, F. Hofmann and J.P. Toennies, J. Chem. Phys. 106 (1997) p. 4327.
[135] M.F. Bertino, J.R. Manson, W. Silvestri, J. Chem. Phys. 108 (1998) p. 10239.
[136] M.F. Bertino, A.P. Graham, L.Y. Rusin, J.P. Toennies, J. Chem. Phys. 109 (1998) p. 8036.
[137] G. Boato, P. Cantini, L. Mattera, Jpn. J. Appl. Phys. Suppl. 2 (2) (1974) p. 553.
[138] M.F. Bertino, A.L. Glebov, J.P. Toennies, F. Traeger, E. Pijper, G.J. Kroes and R.C. Mowrey, Phys. Rev. Lett. 81 (1998) p. 5608.
[139] G. Witte and M.F. Bertino, Surf. Sci. 385 (1997) pp. 1984-1989.
[140] M.F. Bertino, S. Miret-Artés, J.P. Toennies and G. Benedek, Surf. Sci. 377 (1997) pp. 714-718.
[141] M.F. Bertino, S. Miret-Artés and J.P. Toennies, Chem. Phys. Lett. 287 (1998) pp. 663-670.
[142] J. Dai and J.C. Light, J. Chem. Phys. 107 (1997) pp. 1676-1679.
[143] B. Hammer, M. Scheffler, K. Jacobsen and J.K. Norskov, Phys. Rev. Lett. 73 (1994) p. 1400.
[144] W.A. Diño, H. Kasai and A. Okiji, Surf. Sci 363 (1996) pp.52-61.
[145] D. C. Harris, G. R. Darling and S. Holloway, Surf. Sci. 433-435 (1999) pp. 838-842.
[146] G.D. Billing. In: C. Cerjan, Editor, Numerical Grid Methods and Their Application to Schrödinger's Equation, Kluwer, Amsterdam (1993).
[147] R. Kosloff. In: C. Cerjan, Editor, Numerical Grid Methods and Their Application to Schrödinger's Equation, Kluwer, Amsterdam (1993), p. 175.
[148]. G.R. Darling and S. Holloway. J. Chem. Phys. 101 (1994), p. 3268.
[149] D.A. McCormack and G.-J. Kroes, Chem. Phys. Lett. (1998) pp. 515-520.
[150] A. Gross and M. Scheffler, Phys. Rev. B 57 (1998) pp. 2493-2506.
[151] Y. Miura. H. Kasai, W.A. Diño and A. Okiji, Surf. Sci. 438 (1999) pp. 254-260.
[152] W.A. Diño, H. Kasai and A. Okiji, Appl. Surf. Sci. 169-170 (2001) pp. 36-41.
[153] Y. Miura, H. Kasai, W.A. Diño and A. Okiji, Surf. Sci. 493 (2001) pp. 298-304.
[154] Y. Miura, W.A. Diño, H. Kasai and A. Okiji, Surf. Sci. 482-485 (2001) pp. 306-311.
[155] S. Thareja and N. Sathyaamurthy, J. Indian Chem. Soc. 66 (1989) pp. 596-598.
[156] D. Bejan, G. Raesev, and M. Monnerville, Surf. Sci. 470 (2001) pp. 293-310.
[157] B. Jackson and D. Lemoine, J. Chem. Phys. 114 (2001) pp. 474-482.
[158] D. Lemoine and B. Jackson, Computer Physics Communication 137 (2001) pp. 415-426.
[159] E. Pijeper, M.F. Somers, G.J. Kroes, R.A. Olsen, E.J. Baerends, H.F. Busnengo, A. Salin and D. Lemoine, Chem. Phys. Lett., 347 (2001) pp. 277-284.
[160] W.A. Diño, K. Fukutani, T. Okano and H. Kasai, A. Okiji, D. Farías and K.-H. Rieder, to be published in the Journal of Physical Society of Japan Vol. 70, No. 12 (December 2001).

Legends of figures

Figure 1 Probability density functions (PDF) of He-W(112) scattering propagation in the momentum space by colour scale technique. P_x and P_z are the momentum in direction *x* and *z*, respectively. Atomic units are used. (A) PDF is at the beam source region (initial state). (B) - (H) PDF propagates in the interaction region. (I) PDF is at the detector region (final state).

Figure 2 Probability density functions (PDF) in the case of different relative velocity spreads (RVS) of initial wave function by 3D rendering technique. P_x and P_z are the momentum in direction *x* and *z*, respectively. Atomic units are used. (A) RVS is 0 and 5% in direction *x* and *z*, respectively. (B) RVS is 5% in the both directions. (C) RVS is 13% in both directions. (D) RVS is 80% in both directions.

Figure 3 Probability density functions (PDF) in the case of different lattice constants by 3D rendering technique. P_x and P_z are the momentum in direction *x* and *z*, respectively. The relative velocity spread of initial wave function is 5% in both directions. (A) Lattice constant is 5.18 (a.u.). (B) Lattice constants is 10 (a.u.). (C) Lattice constant is 13 (a.u.). (D) Lattice constant is 20 (a.u.). Atomic units are used.

Figure 4 Animation by isosurface technique in real space. The isosurface value is approximately 5% to the maximum of PDF at the initial time. Isosurfaces of PDF are rendered as a function of time in order of abc. (A) Initial wave function. (B)-(H) Interaction region. (I) Final state. An isosurface of interaction potential is also shown.

Figure 5 Animation by window technique with colour scale in the momentum space. Slices of PDF parallel to the periodic surface - near the interaction region as the time progresses - are rendered. P_x and P_y are moment in the direction *x* and *y*, respectively. (A) Wave packet has just reached the window. (B-H) Wave packet is in the interaction region. (I) Wave packet has just left behind the window. Atomic units are used.

Figure 6 He resonant adsorption on He-Rh(311) scattering by window technique with 3D rendering. Atomic units are used. Probability density function (PDF) split into slices parallel to the solid surface. P_x and P_y are the moment in the direction *x* and *y*, respectively. (A) and (B) PDFs are shown in the real space and in the momentum space, respectively when the wave packet is near the classical turning point ($< z >= 2.62$ a.u., *z=2.62*). The radius of the circle in the origin is 3.74 (a.u.). (C) and (D) PDFs are shown in the real and the momentum space when the wave packet is at the detector region. The radius of the circle in the origin is 3.74 (a.u.).

Figure 7 Cumulative probability function (CPF) of He probability density function (PDF) in case of He scattering on W(112) model surface. Thick solid line is the theoretical χ_2^2 law. Filled dots show the CPF from TDWP model

calculations at the detector region after the scattering process. PDF is equal to $\left|\Psi(\mathbf{r},t)\right|^2$, where **r** is the position and *t* is the time.

Figure 1

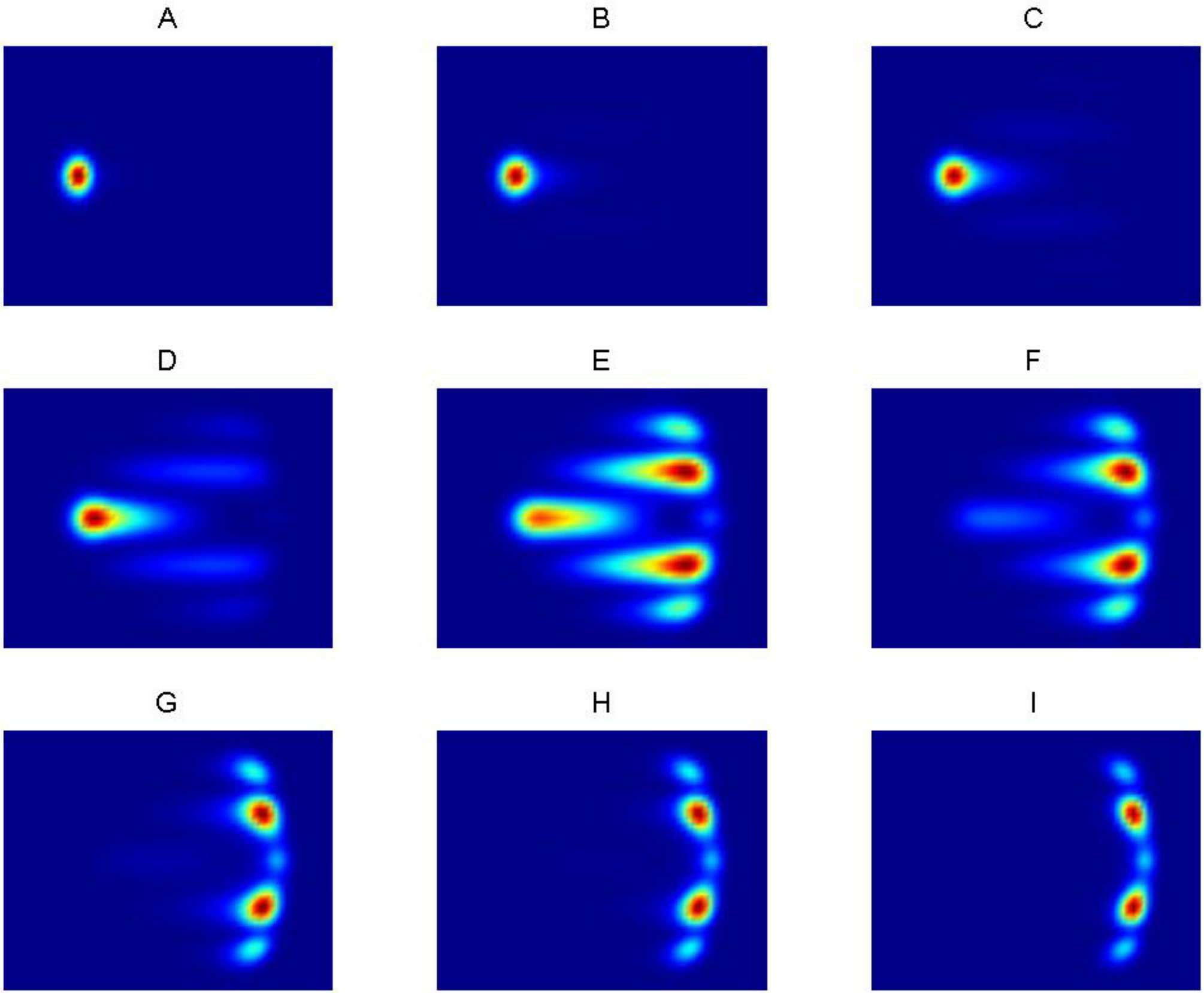

A

B

Figure 2

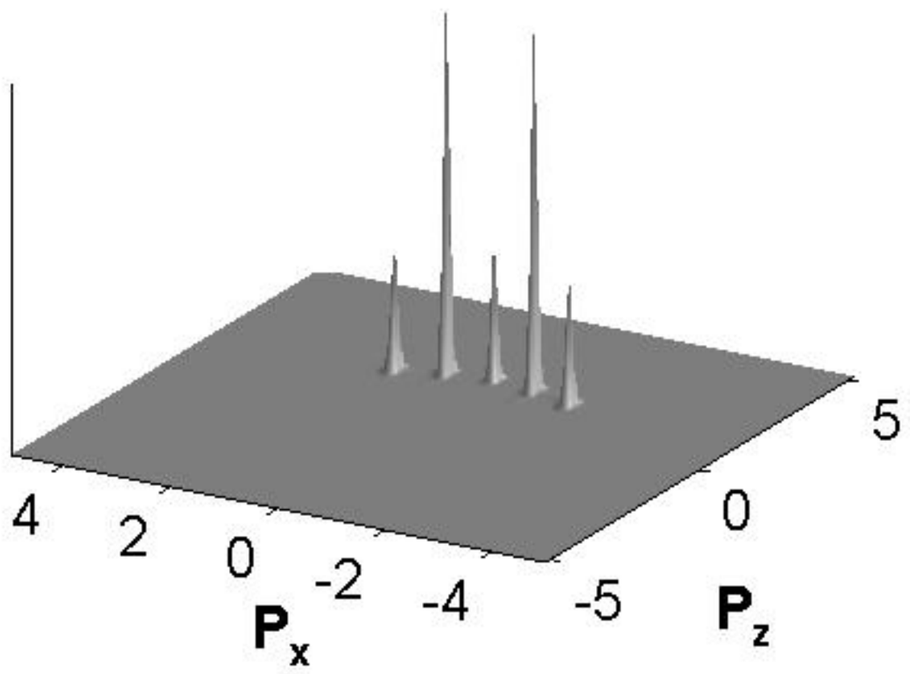

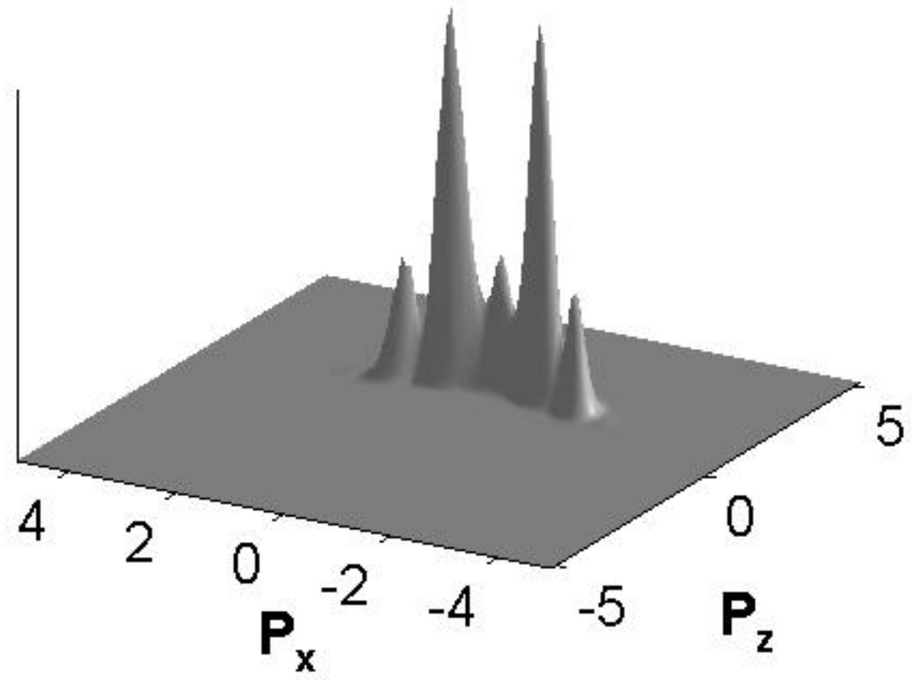

C

D

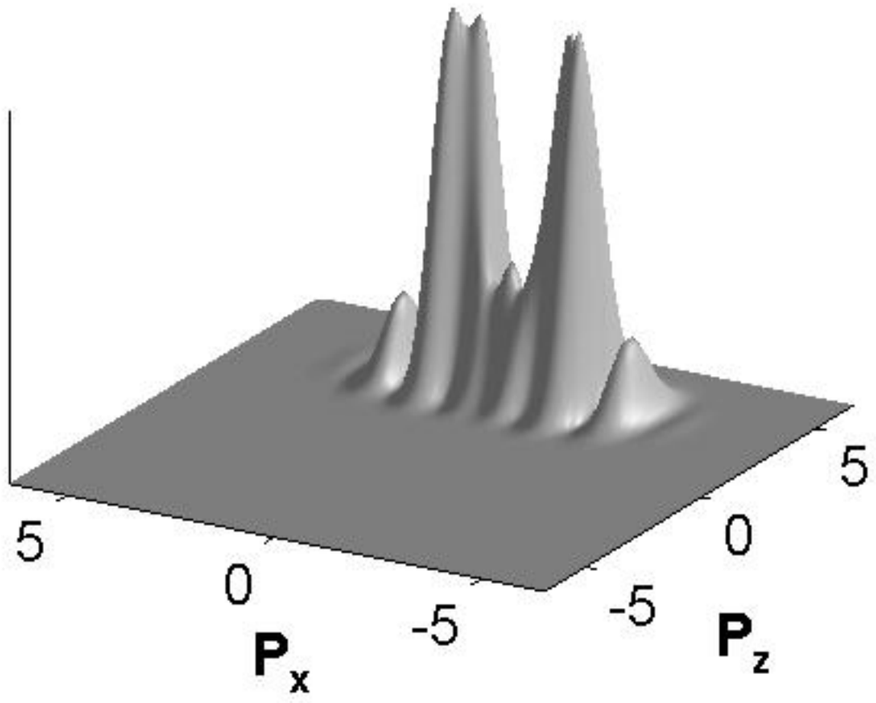

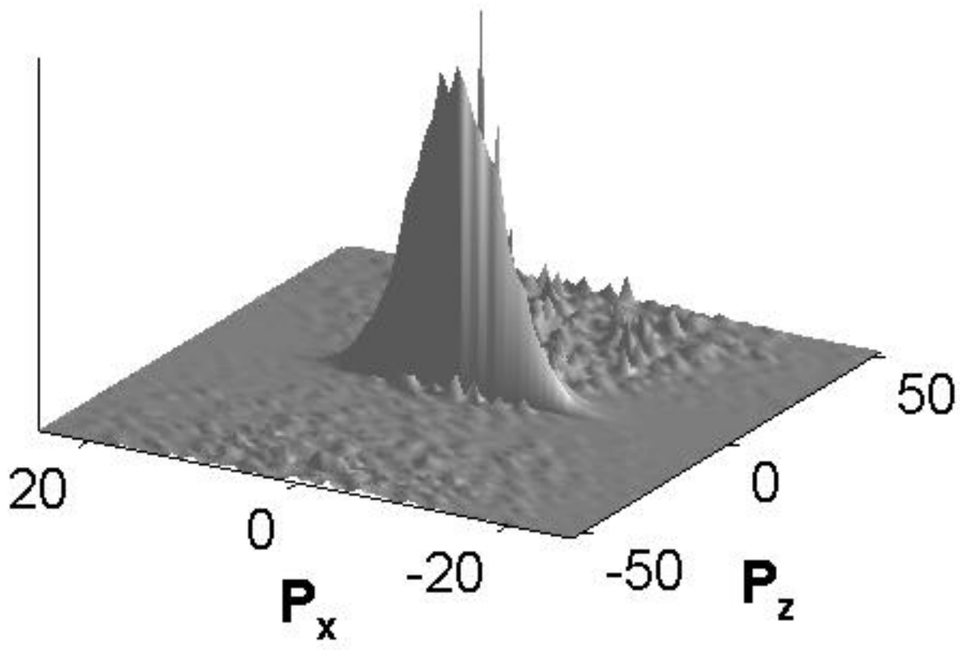

A

B

Figure 3

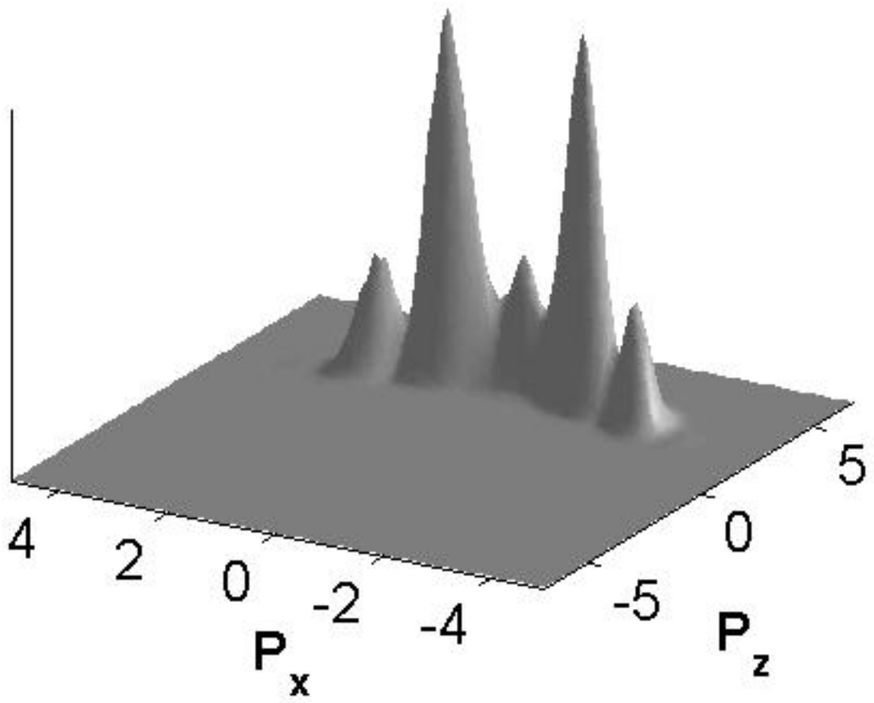

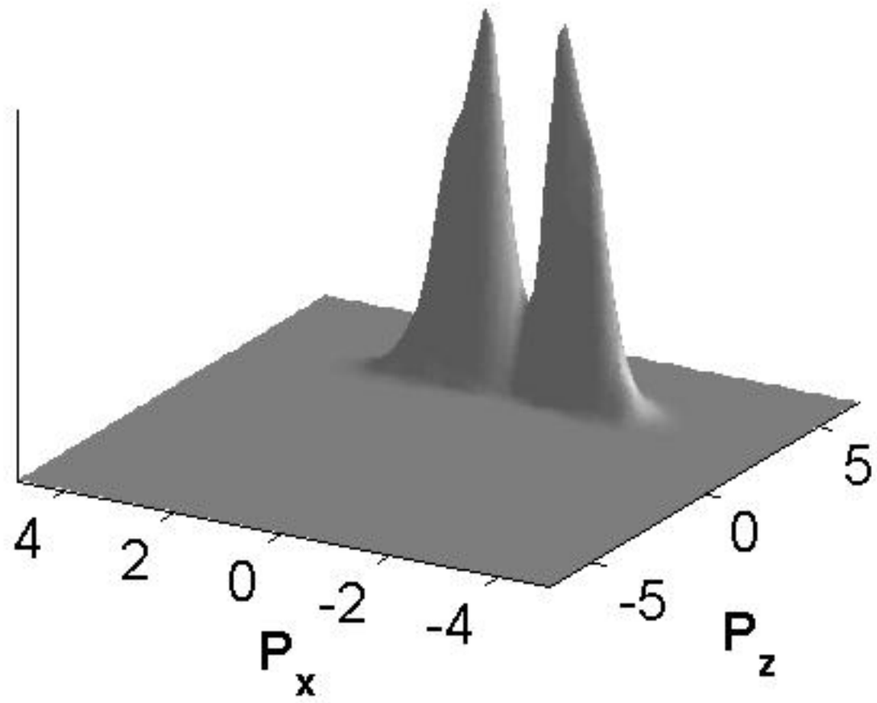

C

D

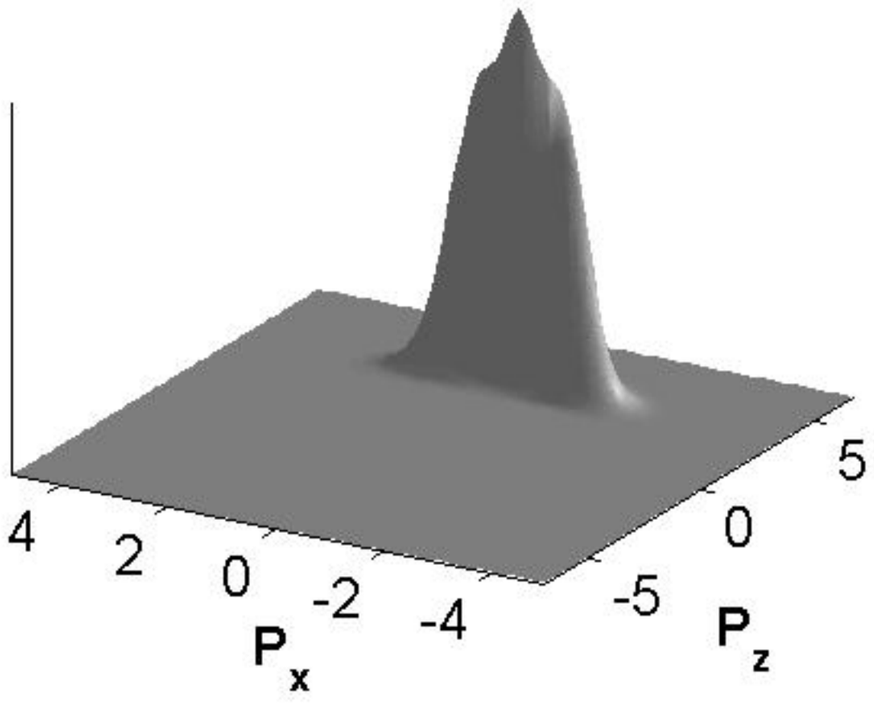

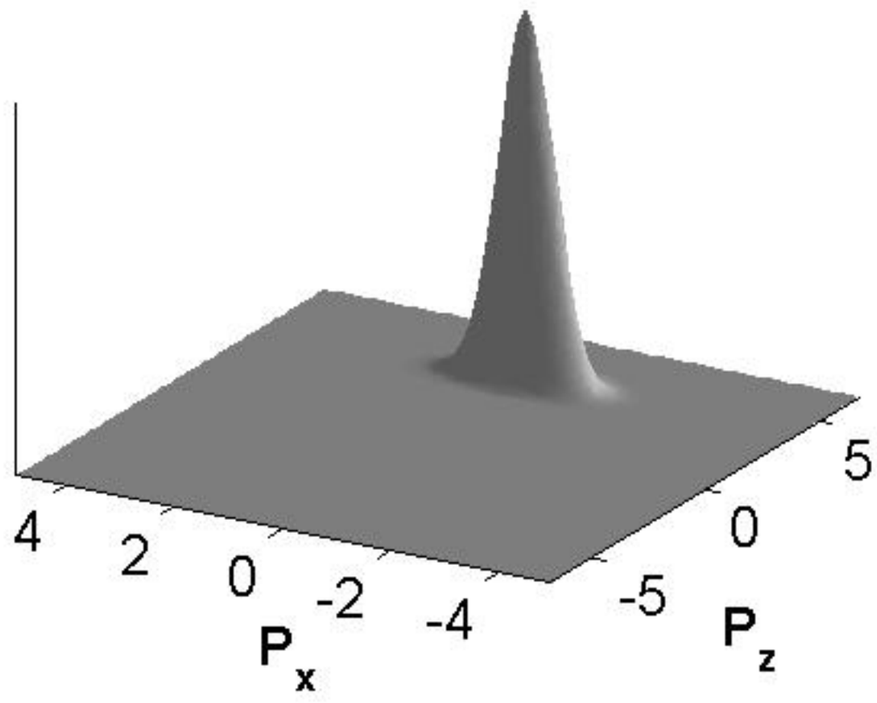

A

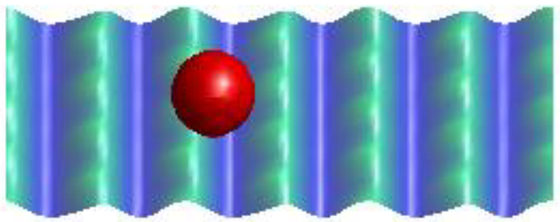

B

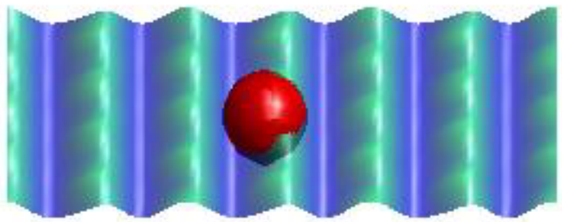

C

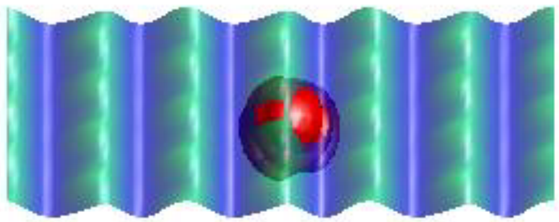

D

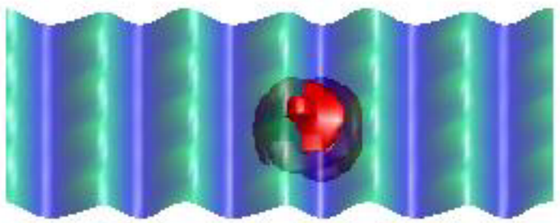

E

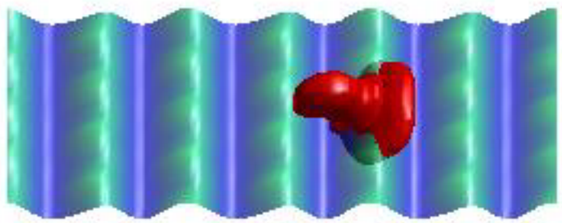

F

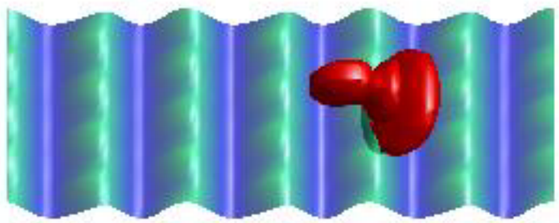

Figure 4

G

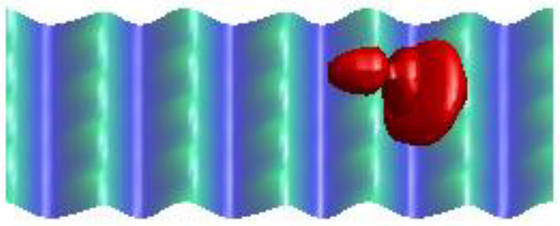

H

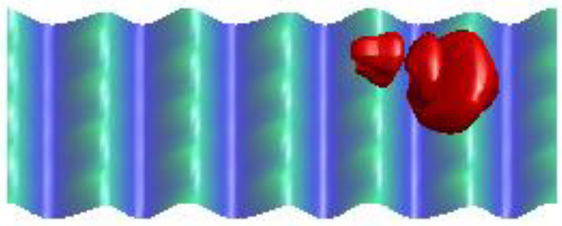

I

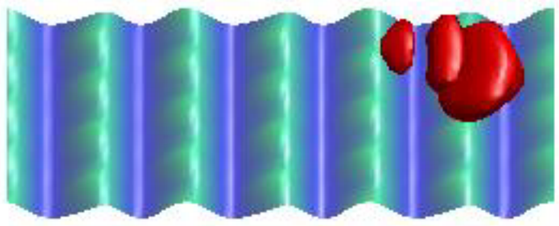

Figure 5

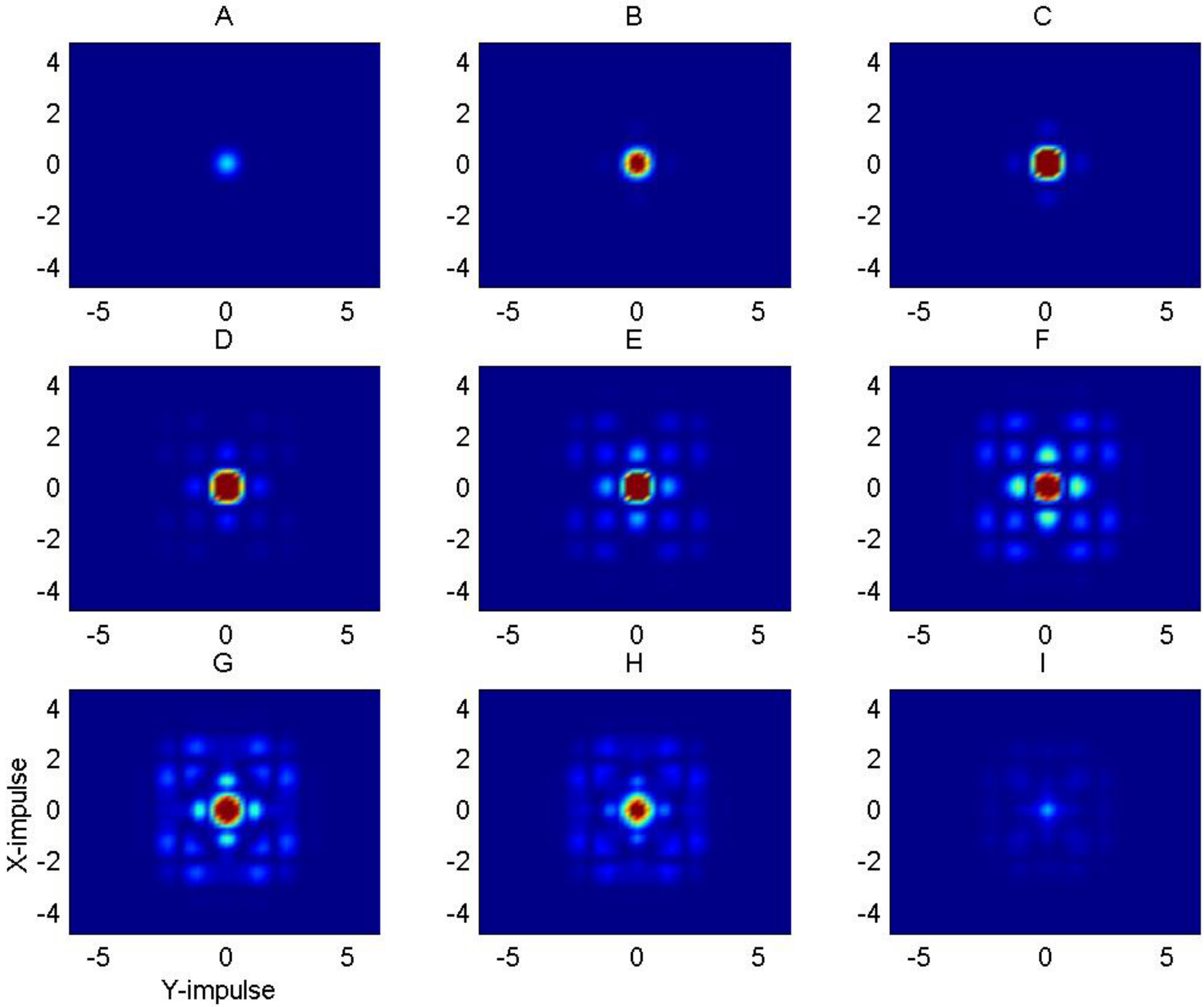

Figure 6

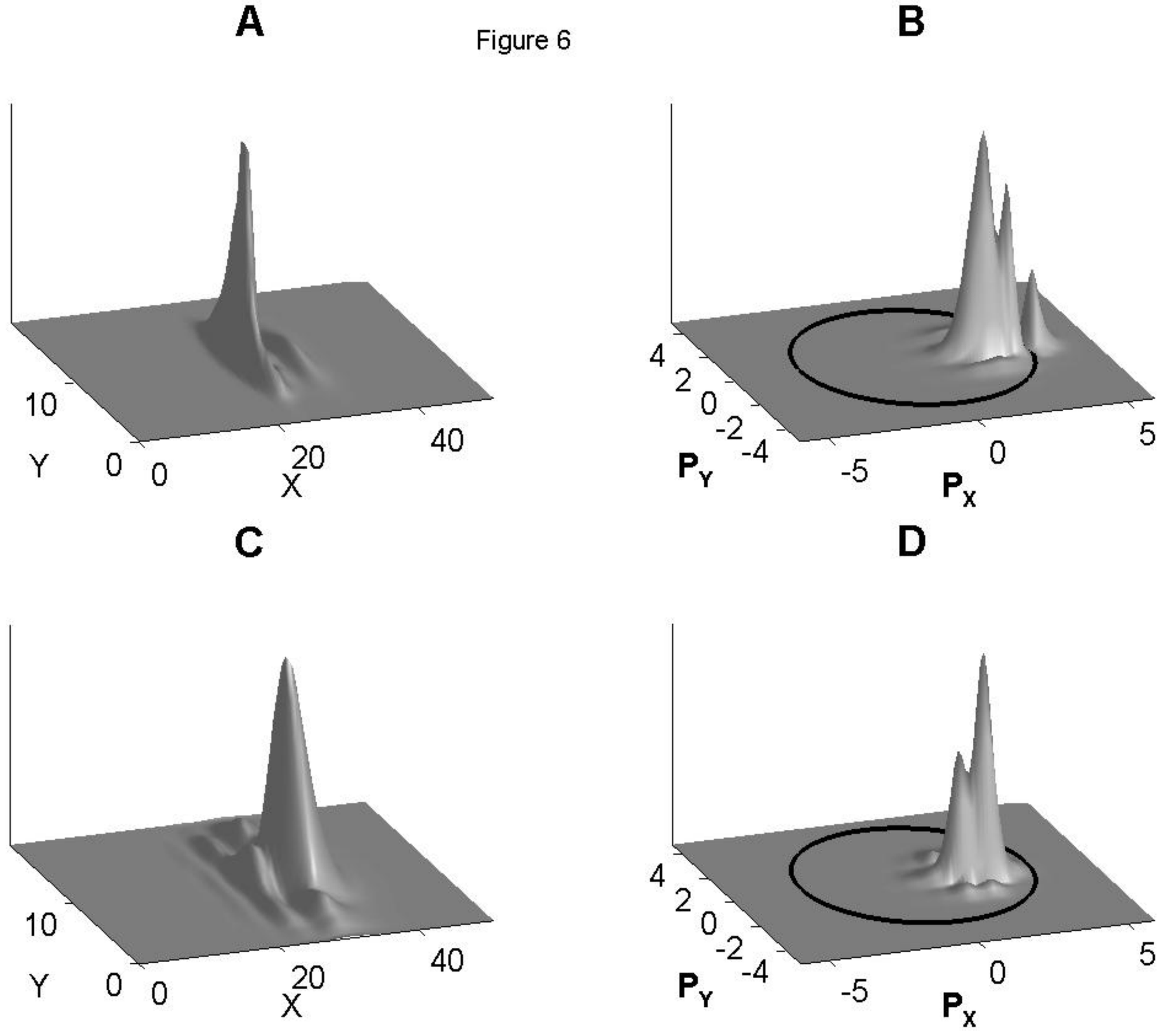

Figure 7

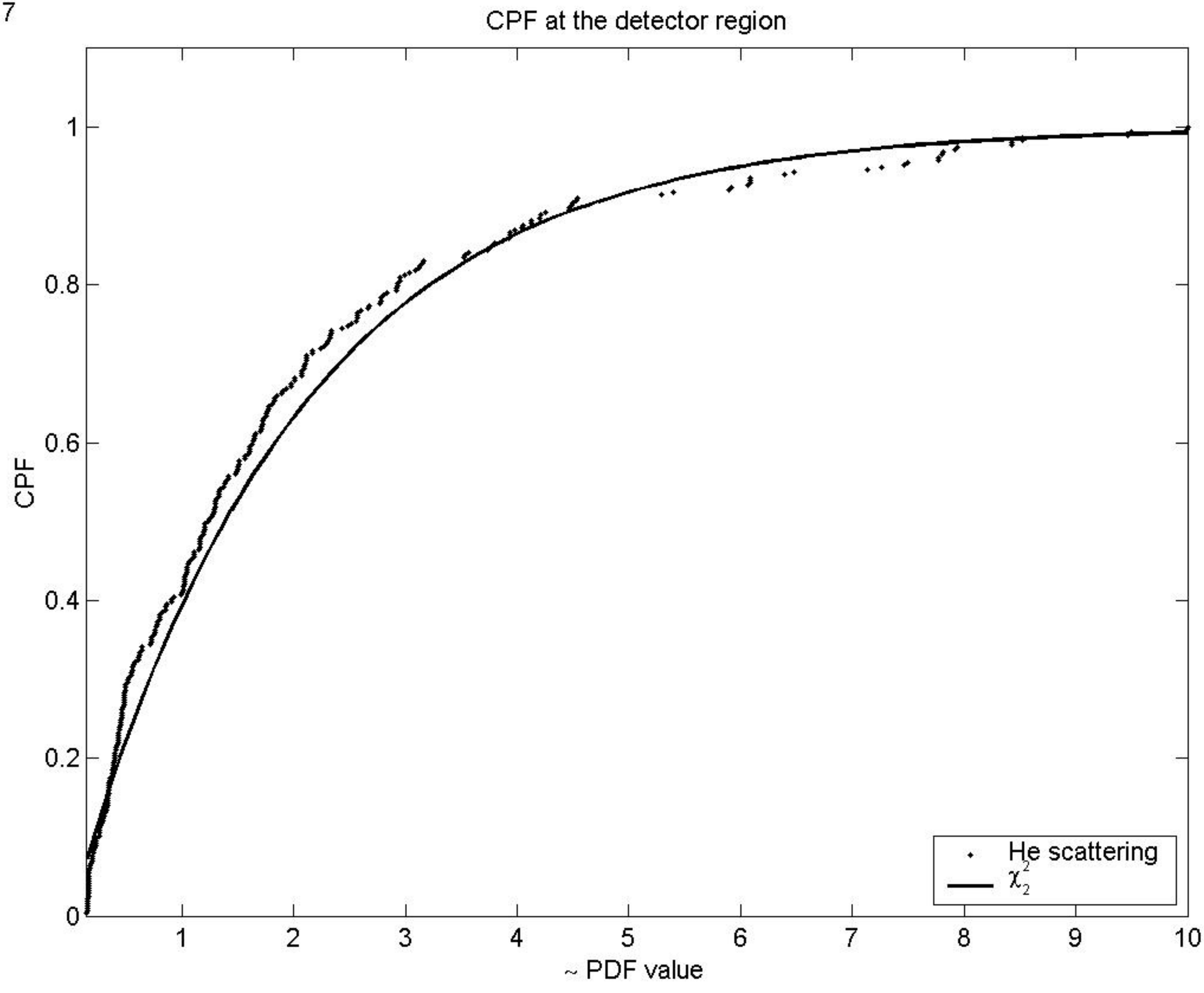
CPF at the detector region
CPF
~ PDF value
He scattering
χ^2_2
0
0.2
0.4
0.6
0.8
1
1
2
3
4
5
6
7
8
9
10